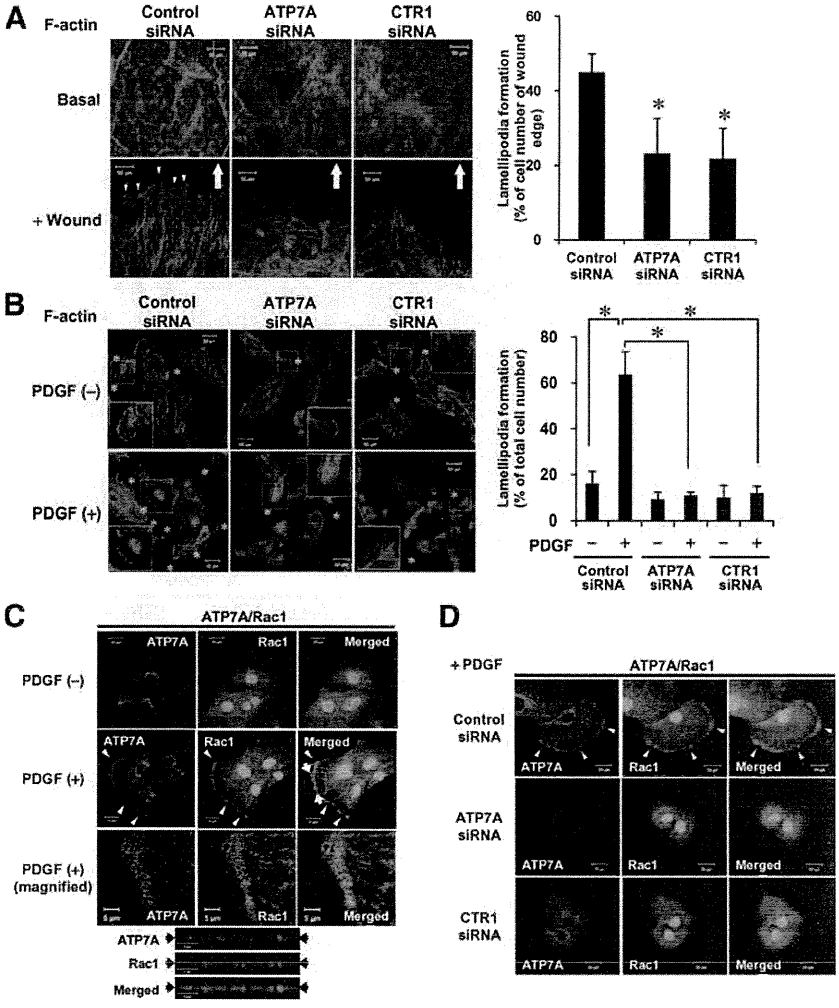

Figure 3. ATP7A is involved in PDGF-stimulated lamellipodia formation and Rac1 translocation in a CTR1-dependent manner in VSMCs. A and B, RASMs transfected with control siRNA or CTR1 siRNA or ATP7A siRNA were stimulated with wound scratch **(A)** or 50 ng/mL PDGF **(B)** as described for Figure 2, and cells were stained for phalloidin to visualize lamellipodia formation. Cells with lamellipodia formation were expressed as percentage of cell number of wound edge **(A)** or total cell number **(B)** (means±SD, n=3). In **B**, cells in boxes are magnified in **insets. Small white arrowheads** point to the leading edge, and **large arrows** point to direction of migration. *$P<0.05$ vs control siRNA-treated cells. **C and D**, RASMs stimulated with or without PDGF as described above and costained with anti-ATP7A antibody **(red)** and anti-Rac1 antibody **(green)**. In **D**, RASMs were transfected with control siRNA or CTR1 siRNA or ATP7A siRNA as described. All fluorescence images were taken at 5 different fields/well, and the cell images are representative of >3 different experiments.

precipitation analysis showed that ATP7A associated with Rac1 in the basal state, which was further enhanced after PDGF stimulation (Online Figure IV, C), suggesting that ATP7A recruits Rac1 to the lipid rafts via binding to Rac1 in response to PDGF directly or indirectly. Furthermore, Rac1 trafficking to the leading edge was inhibited by either ATP7A or CTR1 siRNA (Figure 3D). Thus, the copper transporter ATP7A is involved in PDGF-stimulated translocation of Rac1 to the leading edge, but not Rac1 activation, in a CTR1-dependent manner, which may contribute to lamellipodia formation and VSMC migration.

ATP7A Colocalizes With PDGFR at the Leading Edge in a CTR1-Dependent Manner in PDGF-Stimulated VSMCs

Because we found that ATP7A is a downstream mediator for PDGFR signaling linked to VSMC migration, we next examined the relationship between ATP7A and PDGFR in PDGF-stimulated VSMCs. Immunofluorescence analysis showed that ATP7A colocalized with PDGFR at the leading edge after PDGF stimulation (Figure 4A). Of note, both CTR1 and ATP7A siRNAs inhibited PDGF-induced ATP7A movement to the leading edge without affecting PDGFR localization (Figure 4B). Coimmunoprecipitation analysis further confirmed that PDGF stimulation promoted PDGFR association with ATP7A, which was somewhat inhibited by CTR1 siRNA (Figure 4C). Under this condition, PDGF-induced PDGFR autophosphorylation was not affected by CTR1 siRNA (Figure 4C). Taken together, these results suggest that PDGF stimulation induces colocalization and association of ATP7A with PDGFR at the leading edge in a CTR1-dependent manner, and that CTR1-ATP7A pathway is downstream of PDGFR activation.

PDGF Promotes ATP7A Recruitment to the Caveolae/Lipid Rafts, Where PDGFR, Rac1, and CTR1 Are Localized, in a CTR1-Dependent Manner

To gain further insight into the subcellular compartments in which ATP7A is localized, we performed detergent-free sucrose gradient fractionation in VSMCs, as previously described.[32] Western analysis of sequential fractions from the gradient showed that ATP7A was found in both caveolin-enriched lipid rafts fractions and noncaveolae/lipid rafts fractions which mainly contain paxillin (Figure 5A).[33] By contrast, the CTR1 copper importer was predominantly found in caveolae/lipid rafts. The specificity of the CTR1 antibody, which detects glycosylated CTR1,[34] was verified by CTR1-deficient mouse embryonic fibroblast cells[30] and VSMCs

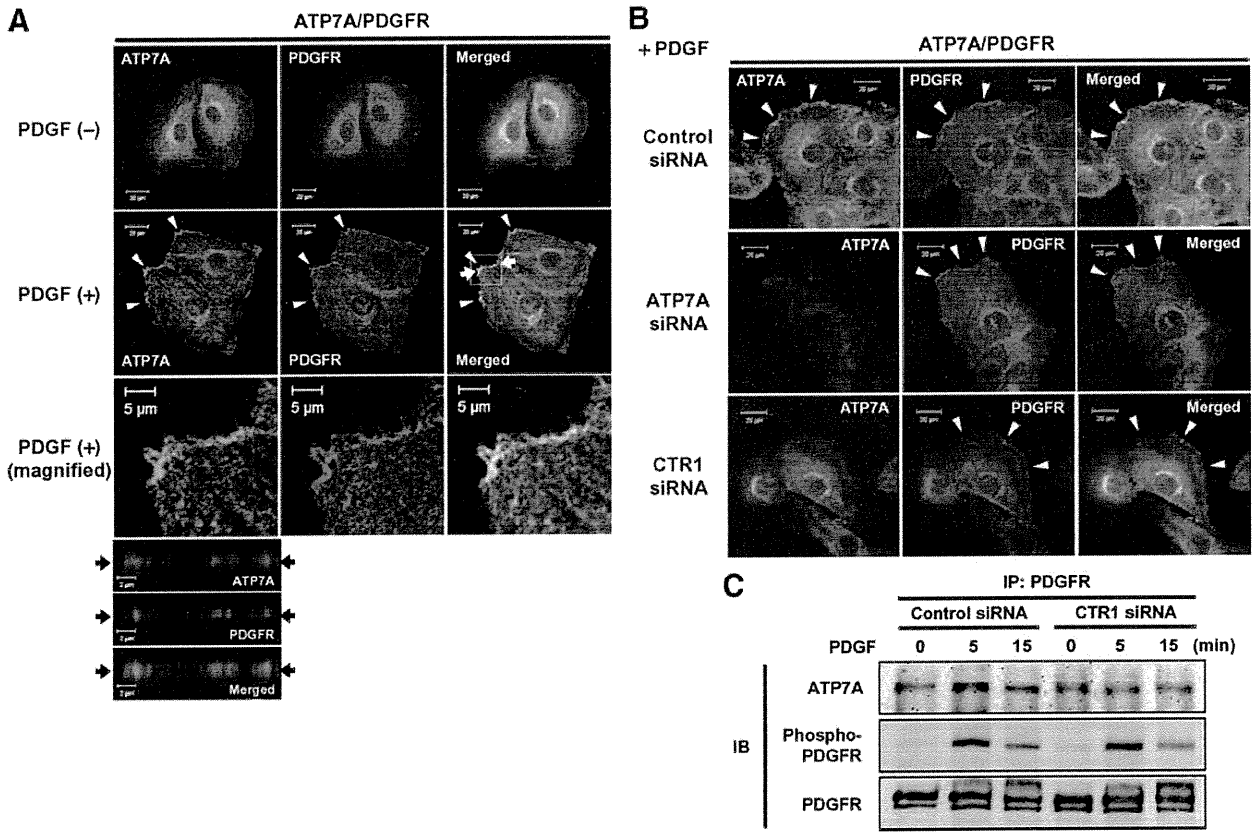

Figure 4. ATP7A colocalizes with PDGFR at the leading edge in a CTR1-dependent manner in PDGF-stimulated VSMCs. A through C, Growth-arrested RASMs were stimulated with 50 ng/mL PDGF for 5 minutes. All fluorescence images were taken at 5 different fields/well, and the cell images are representative of >3 different experiments. **A,** Effect of PDGF on subcellular localization of ATP7A and PDGFR in VSMCs. RASMs were stained with anti-ATP7A antibody **(green)** and anti-PDGFR antibody **(red). B,** Effect of ATP7A or CTR1 siRNA on subcellular localization of ATP7A and PDGFR in PDGF-treated cells. RASMs transfected with CTR1, ATP7A, or control siRNA were double-stained with anti-ATP7A antibody **(green)** and anti-PDGFR antibody **(red). C,** PDGF stimulation promoted PDGFR association with ATP7A in a CTR1-dependent manner. RASMs were transfected with control siRNA or CTR1 siRNA. Growth-arrested confluent monolayer of RASMs was stimulated with 50 ng/mL PDGF for indicated times (min). Lysates were immunoprecipitate (IP) with anti-PDGFR antibody, followed by immunoblot (IB) with ATP7A, phospho-PDGFR, and PDGFR antibody.

transfected with CTR1 siRNA (Online Figure V, A and B). Localization of ATP7A and CTR1 in caveolae/lipid rafts was further confirmed in various VSMCs, including RASM, HASM, and MASM (Online Figure V, C) and using detergent-free OptiPrep gradient cell fractionation (Online Figure V, D). Figure 5B shows that PDGF stimulation for 5 minutes promoted recruitment of ATP7A, CTR1 and Rac1 to the caveolae/lipid rafts fractions without affecting PDGFR localization, which was associated with an increase in PDGFR phosphorylation in these fractions. Significantly, CTR1 siRNA prevented PDGF-induced translocation of ATP7A and Rac1 to the caveolae/lipid rafts without affecting PDGFR phosphorylation (Figure 5B). These suggest that PDGF-induced PDGFR autophosphorylation occurs in caveolae/lipid rafts, which in turn promotes recruitment of ATP7A and Rac1 to these specialized microdomains where PDGFR is localized, in a CTR1-dependent manner.

ATP7A Is Translocated to the Lipid Rafts Localized at the Leading Edge in PDGF-Stimulated VSMCs

Lipid rafts have been shown to be localized at the leading edge during cell migration.[35] We thus examined the spatial relationships among ATP7A, lipid rafts and leading edge after PDGF stimulation using immunofluorescence analysis. As shown in Figure 5C and Online Figure VI (B), ATP7A colocalized with cholera toxin subunit B (CTxB), a lipid raft marker,[35] at the leading edge in PDGF- and wound scratch-stimulated VSMCs. Furthermore, CTxB accumulated and colocalized with F-actin at the leading edge in actively migrating VSMCs (Online Figure VI, A and C). Disruption of lipid rafts by cholesterol binding reagent, methyl-β-cyclodextrin, completely abrogated the ATP7A localization at the leading edge and CTxB staining (Figure 5D) as well as lamellipodia formation (Online Figure VI, A). These results suggest that PDGF stimulates translocation of ATP7A to the lipid rafts localized at the leading edge, thereby promoting lamellipodia formation.

PDGF Stimulation Reduces Copper Content in Caveolae/Lipid Raft Fractions in VSMCs

Because ATP7A is involved in exporting copper to the extracellular space, we next examined the effects of PDGF on copper levels in VSMCs. At first, we performed ^{64}Cu

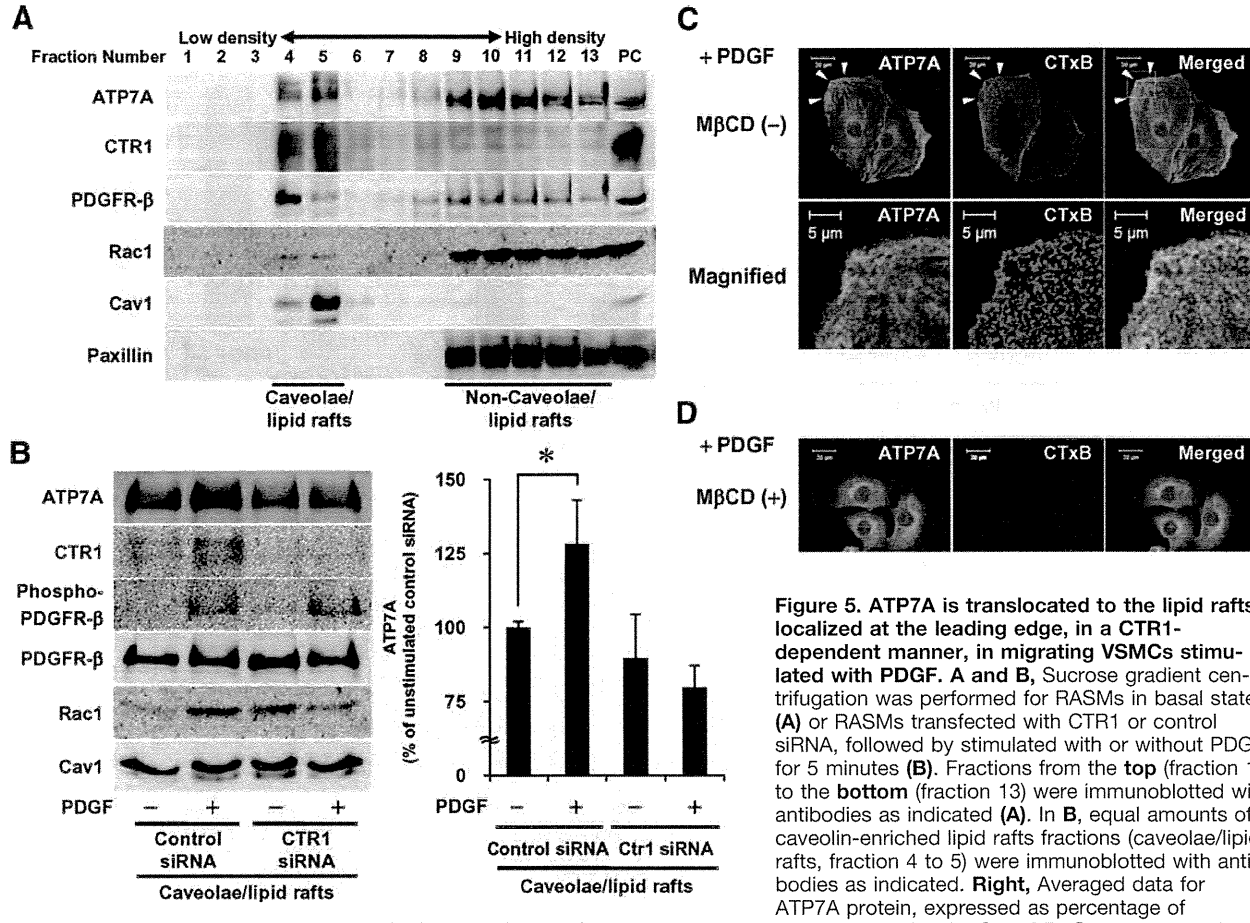

Figure 5. ATP7A is translocated to the lipid rafts localized at the leading edge, in a CTR1-dependent manner, in migrating VSMCs stimulated with PDGF. A and B, Sucrose gradient centrifugation was performed for RASMs in basal state **(A)** or RASMs transfected with CTR1 or control siRNA, followed by stimulated with or without PDGF for 5 minutes **(B)**. Fractions from the **top** (fraction 1) to the **bottom** (fraction 13) were immunoblotted with antibodies as indicated **(A)**. In **B**, equal amounts of caveolin-enriched lipid rafts fractions (caveolae/lipid rafts, fraction 4 to 5) were immunoblotted with antibodies as indicated. **Right,** Averaged data for ATP7A protein, expressed as percentage of unstimulated, control siRNA-treated VSMCs (means±SD, n=3). *$P<0.05$ vs control siRNA-treated cells. **C and D,** Growth-arrested RASMs were treated with **(C)** or without **(D)** 10 mmol/L methyl-β-cyclodextrin for 2 hours and stimulated with 50 ng/mL PDGF for 5 minutes. Cells were costained with anti-ATP7A antibody **(green)** and Alexa 555–CTxB **(red)**. All fluorescence images were taken at 5 different fields/well and are representative of >3 different experiments.

efflux and ^{64}Cu uptake experiments in cultured VSMCs and found that PDGF stimulation had no effects on either response (Online Figure VII). Similarly, ICP-MS analysis of total cell lysates of VSMCs also showed that copper contents were not changed after PDGF stimulation (Figure 6A). Because ATP7A is recruited to the caveolae/lipid rafts in response to PDGF, we next measured the copper content in the lipid rafts and nonlipid raft fractions. Intriguingly, we found that the caveolae/lipid rafts fraction contains much higher amounts of copper than nonlipid raft fractions in the basal state (Figure 6B). Moreover, PDGF stimulation significantly reduced copper content in caveolae/lipid rafts in an ATP7A-dependent manner (Figure 6C and Online Figure VIII). These results suggest that PDGF-induced recruitment of ATP7A to the lipid rafts may contribute to copper export to the extracellular space in these specialized microdomains. This was not detected by global measurements of ^{64}Cu efflux and ^{64}Cu uptake in whole cells. The plasma membrane localization of ATP7A and CTR1 in PDGF-stimulated VSMCs was confirmed by using cell surface biotinylation assays (Online Figure IX).

We next examined whether PDGF-induced decrease in copper content in caveolae/lipid rafts may reflect the secretion of copper-binding proteins, such as Pro-LOX which obtain copper from ATP7A. We found that pro-LOX was localized in caveolae/lipid rafts in the basal state, and PDGF stimulation promoted the reduction of pro-LOX level in an ATP7A dependent manner in these fractions (Figure 6D and 6E; Online Figure X). After secretion, Pro-LOX is processed to a mature active nonglycosylated LOX and a glycosylated propeptide LOX-PP.[22,23] Of note, LOX and LOX-PP were not found in caveolae/lipid rafts in the basal state or after PDGF treatment (Figure 6D and 6E). Taken together, these findings suggest that PDGF-stimulated ATP7A recruitment into the caveolae/lipid rafts may be required for the secretion of copper-dependent enzymes such as pro-LOX localized in these specific compartments.

It has been reported that ATP7A is involved in LOX activity[17,36] and that LOX activity is involved in PDGF-induced VSMC migration[24] in addition to its effect on extracellular matrix remodeling. We thus examined whether LOX activity is involved in copper transporter ATP7A-dependent PDGF-induced VSMC migration. ATP7AsiRNA significantly inhibited LOX activity in VSMCs treated with PDGF (Online Figure XII, A). Furthermore, treatment of a specific chemical LOX activity inhibitor, βaminopropion-

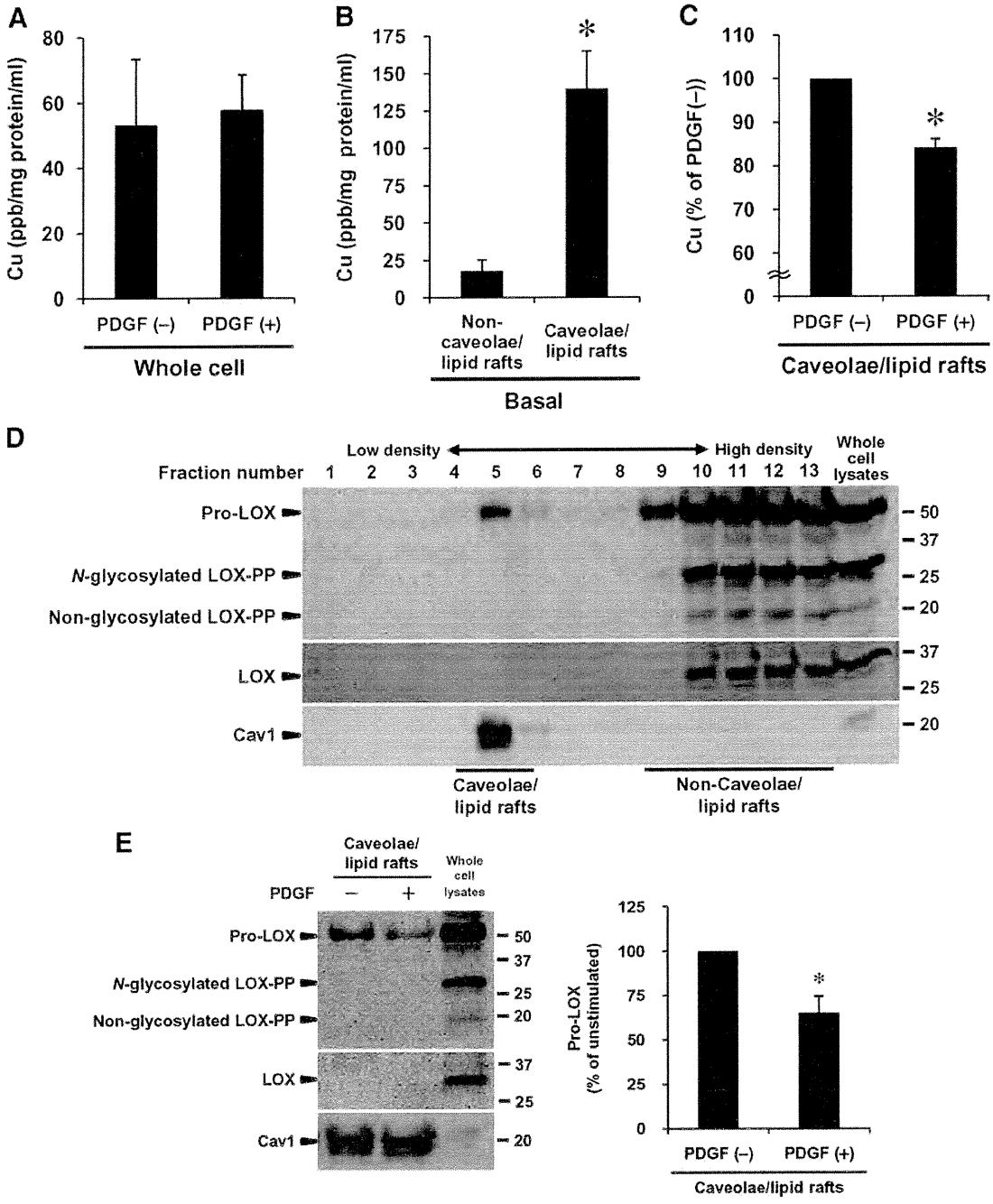

Figure 6. PDGF stimulation reduces copper content and Pro-LOX in lipid rafts fractions in VSMCs. A through C, Copper contents were measured by ICP-MS in whole cells **(A)** or caveolae/lipid rafts or noncaveolae/lipid rafts **(B and C)** in RASMs with or without PDGF stimulation for 5 minutes. Equal amounts of proteins in caveolae/lipid rafts (fractions 4 to 5) or noncaveolae/lipid rafts (fractions 9 to 13) were obtained by sucrose gradient fractionation as described for Figure 5. *$P<0.05$ vs nonlipid rafts or unstimulated cells (means±SD, n=3). **D,** Identification of Pro-LOX, but not LOX, in caveolae/lipid rafts in VSMCs. RASMs were fractionated by sucrose gradient centrifugation, followed by immunoblotted with anti–LOX-PP (which detects both Pro-Lox and LOX-PP), anti-LOX, or anti–caveolin-1 antibodies. **E,** Effect of PDGF treatment on Pro-LOX level in caveolae/lipid rafts fractions in VSMCs. Equal amounts of proteins in caveolae/lipid rafts (fractions 4 to 5) were immunoblotted with anti–LOX-PP, -LOX, or –caveolin-1 antibodies in RASMs with or without 50 ng/mL PDGF for 5 minutes.

itrile (BAPN), significantly inhibits PDGF-induced VSMC migration (Online Figure XII, B), which is consistent with the report by Lucero et al.[24] These findings suggest that LOX activity is involved in PDGF-induced, ATP7A-dependent VSMC migration.

ATP7A Is Upregulated in Neointimal Formation in Response to Vascular Injury In Vivo

To determine the functional significance of ATP7A in VSMC migration in vivo, we examined the role of ATP7A in neointimal formation using a mouse wire injury model.

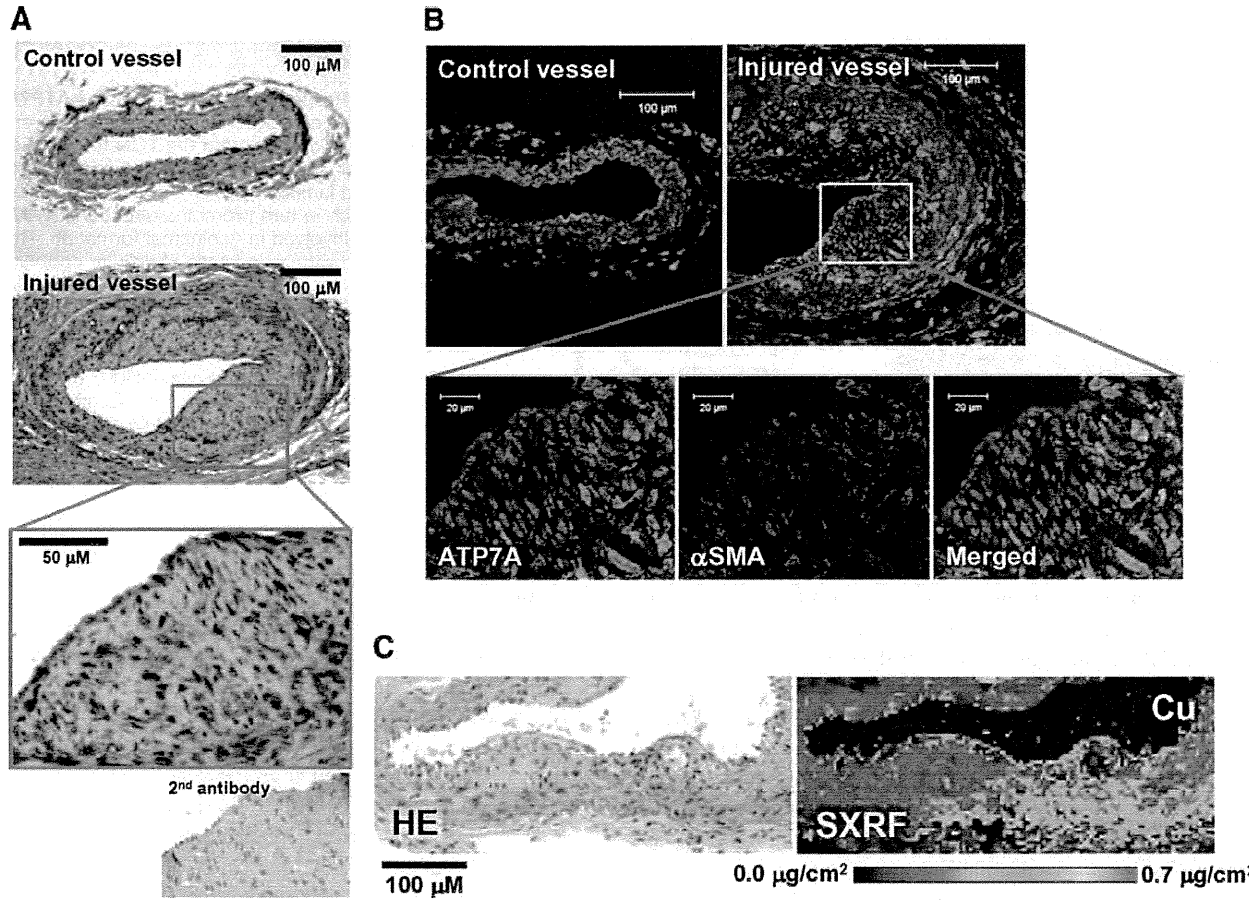

Figure 7. ATP7A is involved in neointimal formation in response to vascular injury in vivo. A and B, ATP7A is highly expressed in neointimal VSMCs of wire-injured carotid arteries of ApoE-deficient atherosclerotic mice. Immunohistochemical **(A)** or immunofluorescence **(B)** analysis for uninjured (control) or injured (4 weeks after) carotid artery stained with anti-ATP7A antibody **(A)**; or costained with anti- ATP7A **(green)** and α-smooth muscle actin **(red)** antibodies **(B)**. **C,** X-ray fluorescence microscopy scans of the neointima of wire-injured carotid arteries. Areas of neointimal lesions were identified by hematoxylin/eosin staining **(left)**. X-ray fluorescence microscopy scans (1 to 2 seconds per pixel) were performed in paraffin-embedded tissue **(right)**. Map of Cu shows areas of the lowest to the highest content scaled to a rainbow color **(bottom)**. Copper accumulation in neointimal lesions is shown in **white arrow**. The minimal and maximal Cu content displayed in micrograms per square centimeter is shown in the image.

Immunohistochemical analysis showed that ATP7A protein expression was robustly increased in neointimal VSMC and endothelial cells lining the lumen in the injured vessel of ApoE-deficient atherosclerotic mice (Figure 7A). Immunofluorescence analysis demonstrated that ATP7A was colocalized with α-smooth muscle actin, a VSMC marker, in the neointima formed in response to injury (Figure 7B). We next examined if induction of ATP7A precedes VSMC migration after injury to address the cause-effect of ATP7A in VSMC migration in vivo. As shown in Online Figure XI, we observed increase in ATP7A expression at 3 days after wire injury in the vessels of ApoE-deficient atherosclerotic mice, whereas there was no VSMC migration and neointima formation at this time point as reported by Linder et al.[37] Thus, these findings suggest that ATP7A expression is increased before the onset of VSMC migration following vascular injury and this upregulation is also observed in neointimal VSMCs. Finally, we examined spatial distribution of copper in neointima using synchrotron-based x-ray fluorescence microscopy (SXFM).[28] As shown in Figure 7C, copper accumulation was observed at neointimal lesions in wire injury model. These results suggest that ATP7A may be involved in neointima formation in response to vascular injury in vivo.

Discussion

A role for copper in tissue repair, neointima thickening and atherosclerosis has been suggested; however, the underlying detailed mechanisms remain unknown.[3–7,9–11] Here we provide novel evidence that the ATP7A copper transporter is involved in PDGF-stimulated VSMC migration, which is critical for neointimal formation and vascular remodeling (Figure 8). We found that stimulation with PDGF promotes ATP7A translocation from TGN to the leading edge. This PDGF-induced ATP7A movement toward the site of actin remodeling is inhibited by cell permeable and impermeable copper chelators as well as depletion of the CTR1 copper importer. It has been shown that relocalization of ATP7A from the Golgi is triggered by increased cytoplasmic copper as well as by estrogen, insulin, NMDA (*N*-methyl-D-aspartate) activation, hypoxia, and cytokines.[2,16,38,39] However, our data are the first demonstration that the ATP7A

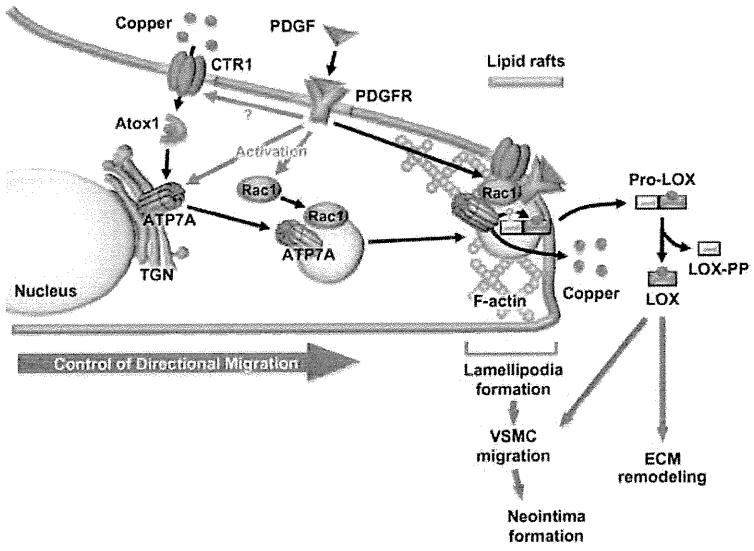

Figure 8. Proposed model for role of ATP7A in PDGF-induced VSMC migration. PDGF promotes ATP7A translocation from the TGN to the lipid rafts, which localize at the leading edge, thereby stimulating lamellipodia formation via recruiting Rac1, which in turn promotes directional VSMC migration involved in neointimal formation. This is associated with a decrease in cellular copper level and secretory copper enzyme prolysyl oxidase (Pro-LOX) at the lipid rafts, which is extracellularly processed and activated by proteolysis to a mature lysyl oxidase (LOX) and a propeptide (LOX-PP), which may promote extracellular matrix (ECM) remodeling and VSMC migration. Secreted copper may also contribute to PDGF-induced cell migration.

copper transporter translocates to the leading edge during growth factor-stimulated cell migration. It has been reported that ATP7A trafficking is in part dependent on its catalytic activity, which requires copper binding to conserved cysteines within its N-terminal region.[17–19] Extracellular copper influx is mainly mediated through CTR1, the copper importer, which is also the major source of "bioavailable" copper for ATP7A via the Atox1 copper chaperone.[29,30] Indeed, Atox1 siRNA prevented PDGF induced ATP7A translocation to the leading edge, suggesting that Atox1 is involved in PDGF-induced translocation of ATP7A (data not shown). Thus, our findings are consistent with the possibility that ATP7A obtains copper via Atox1 by stimulating extracellular copper uptake through CTR1 in response to PDGF, thereby promoting ATP7A trafficking from the Golgi to the leading edge in VSMCs. However, we failed to detect a PDGF-induced increase in ^{64}Cu uptake in whole cell labeling of VSMCs with ^{64}Cu in this study. This may be attributable to the possibility that CTR1-mediated copper uptake occurs in the specific plasma membrane compartment, as discussed below. It is not known how ATP7A is translocated to the leading edge after PDGF stimulation in a copper-dependent manner. Phosphorylation of ATP7A has been shown to be involved in copper-induced relocalization of this protein.[40] Thus, it is possible that PDGF stimulation may induce phosphorylation of ATP7A, which may contribute to its translocation to the leading edge. Taken together, our findings provide a novel linkage between copper homeostasis and PDGF-induced VSMC migration.

Migrating cells form protrusions, such as lamellipodia, by reorganizing of the actin cytoskeleton at the leading edge, which plays an important role in cell migration. The small G protein family Rac1 plays a key role in lamellipodia formation[31] and PDGF-stimulated cell migration.[13] In the present study, we demonstrate that ATP7A is involved in PDGF-induced lamellipodia formation and Rac1 translocation to the leading edge without affecting Rac1 activity, in a copper- and CTR1-dependent manner. Coimmunoprecipitation analysis showed that ATP7A associated with Rac1 in the basal state, which was further enhanced after PDGF stimulation (Online Figure IV, C), suggesting that ATP7A recruits Rac1 to the lipid rafts via binding to Rac1 in response to PDGF directly or indirectly. In line with our data, previous reports show that trafficking of ATP7A from the TGN to the cell surface is associated with actin networks and involves Rac1, which is distinct from the major constitutive secretory pathway.[16,41] Of note, PDGF stimulation also promotes colocalization and association of ATP7A with PDGFR at the leading edge. However, CTR1 siRNA prevents ATP7A translocation to the leading edge without affecting PDGFR localization and its autophosphorylation. These results suggest that CTR1-ATP7A-Rac1 pathway is downstream of PDGFR activation involved in lamellipodia formation and VSMC migration.

Caveolae and lipid rafts are specialized membrane microdomains that are highly enriched in cholesterol and sphingolipids and function as platforms for assembly of signaling molecules including G proteins and receptors involved in various functions.[35] In chemoattractant-stimulated cancer cells, lipid rafts are accumulated at the leading edge.[35] Using sucrose gradient fractionation, the present study shows that PDGF stimulation promotes recruitment of ATP7A and Rac1 to the caveolae/lipid rafts where CTR1 and PDGFR are localized, in a CTR1-dependent manner. By contrast, CTR1 siRNA has no effect on PDGF-induced PDGFR tyrosine phosphorylation as well as localization of caveolin-1 and PDGFR in caveolae/lipid rafts fractions, suggesting that the structure of caveolae/lipid rafts is intact in CTR1 depleted VSMCs. Immunofluorescence analysis also reveals that the marker for lipid rafts, CTxB,[35] colocalizes with ATP7A at the leading edge of migrating VSMCs. We confirmed the plasma membrane localization of ATP7A and CTR1 in PDGF-stimulated VSMCs using cell surface biotinylation assays. PDGF-induced Rac1 translocation to the lipid rafts has been reported in Rat-1B cells[13]; however, our data provides the first evidence that copper transporters CTR1 and ATP7A are localized in these specialized plasma membrane microdo-

mains. Functional significance of copper-dependent ATP7A trafficking into lipid rafts is demonstrated by showing that disruption of lipid rafts by the cholesterol-binding reagent, methyl-β-cyclodextrin, completely inhibits PDGF-induced ATP7A translocation to the leading edge as well as lamellipodia formation. Moreover, PDGF stimulation rapidly decreases the copper content of caveolae/lipid rafts in an ATP7A-dependent manner, as measured by ICP-MS. This PDGF effect is associated with recruitment of ATP7A to lipid rafts where CTR1 is predominantly found. The rapid kinetics of ATP7A is reminiscent of copper-induced ATP7A recruitment into a fast-recycling pool located in close proximity with the plasma membrane.[2,16,17,42] Hung YH et al have reported that the copper content of lipid rafts is paradoxically decreased, when cytoplasmic copper is increased.[43] Thus, it is conceivable that PDGF may stimulate copper uptake via CTR1 to provide copper to ATP7A, which in turn promotes ATP7A translocation from the Golgi to the caveolae/lipid rafts to export copper to extracellular space in the specific compartments. Interestingly, we could not detect any changes in copper levels in response to PDGF in total cell lysates. This may support the suggestion that global measurements of ^{64}Cu efflux and ^{64}Cu uptake in whole cells would fail to detect compartmentalized changes of copper distribution observed in the present study.

The physiological consequence of copper export via ATP7A is not merely the elimination of excess cellular copper, but to supply adequate copper to the developing fetus as gestation progresses,[16] or to provide copper as part of a neuronal protective mechanism.[2] Using SXFM, Finney et al reported that copper is transported from intracellular compartments to the tips of endothelia during capillary growth, which is required for capillary tube formation.[28] In the present study, we demonstrate that the copper-dependent Pro-LOX, which is secreted and activated in the extracellular space,[22] is localized at caveolae/lipid rafts in the basal state. PDGF stimulation significantly reduces Pro-LOX levels in caveolae/lipid rafts fractions in an ATP7A-dependent manner. This may reflect the secretion of pro-LOX after obtaining copper from the recruited ATP7A in these specialized compartments. Importantly, recent evidence suggests that LOX and LOX-PP, both of which are produced from Pro-LOX through proteolysis in the extracellular space, have opposite effects on cell migration.[23–25] Furthermore, and consistent with our results, ATP7A has been shown to deliver copper to some secretory copper enzymes in the post-Golgi vesicles rather than in the TGN, where copper loading normally takes place.[38,44] Taken together, these findings suggest that copper-dependent ATP7A trafficking to lipid rafts in response to PDGF may not simply reflect export copper to the extracellular space, but also facilitate copper-loading to pro-LOX in post-Golgi compartments such as lipid rafts, thereby promoting VSMC migration. To support this, we found that ATP7A siRNA significantly inhibited LOX activity in VSMCs treated with PDGF and that the chemical LOX activity inhibitor β-aminopropionitrile significantly blocked PDGF-induced VSMC migration.

A functional role of the copper transporter ATP7A in VSMC migration in vivo is underscored by upregulation of ATP7A expression and copper accumulation (shown by SXFM) in intimal a-smooth muscle actin positive cells. Of note, ATP7A expression is increased before the onset of VSMC migration after vascular injury and this upregulation was also observed in neointimal VSMCs at later time. These findings suggest that ATP7A may play a role in VSMC migration in vivo. Previous reports indicate that copper plays an important role in various cardiovascular diseases and cancer. High serum copper levels are associated with an increased future risk of coronary heart disease.[4,5,7] Atherosclerotic lesions have higher copper levels than normal tissues.[9] Neointimal thickening after vascular injury is inhibited by copper chelation[11] and increased by copper cuffs and stents.[10] Copper deficiency therapies prevent tumor progression in clinical trials.[3] Interestingly, we found that ATP7A is involved in PDGF-stimulated decrease in copper level and Pro-LOX in caveolae/lipid rafts as well as PDGF-stimulated increase in LOX activity in VSMCs. Furthermore, we showed that inhibition of LOX activity blocks PDGF-induced VSMC migration as reported previously.[24] Given that LOX activity is also essential for vascular extracellular matrix maturation, these results suggest that ATP7A copper transporter may promote extracellular matrix deposition, as well as neointimal formation after vascular injury via regulation of LOX activity.[45] In addition, one of the major copper- and ATP7A-dependent enzymes regulating ROS metabolism is SOD3, but not either SOD1 or SOD2.[21] We thus investigated the contribution of SOD3 but found that SOD3 siRNA had no effect of PDGF-induced directional VSMC migration (Online Figure XII, C). X-ray fluorescence microscopy scans do not clearly show codistribution of copper levels with ATP7A. This may be attributable to the possibility that copper secreted by ATP7A is more widely distributed because of the diffusible nature as ions, and that other copper binding proteins may be involved in neointima formation. Taken together with in vitro data, our findings indicate that upregulation of ATP7A and copper accumulation in neointimal VSMCs may contribute to neointimal formation and vascular remodeling in vivo at least in part by regulating VSMC migration and LOX activity. Because our vascular injury data implicates but does not conclude that ATP7A may play a role in VSMC migration in vivo, further investigation will be required using ATP7A mutant mice[46] in future study.

In conclusion, the present study uncovers a novel function of ATP7A as a regulator for PDGF-induced VSMC migration via recruiting Rac1 to lipid rafts at the leading edge in a copper dependent manner, as well as controlling LOX activity, which may contribute to vascular remodeling (Figure 8). They also indicate an important new role for lipid rafts in organizing the protein components involved in copper homeostasis and signaling. Our findings also provide insight into ATP7A as a potential therapeutic target for various pathophysiologies, such as atherosclerosis, postangioplasty restenosis, diabetes, and cancer, which are associated with dysregulation of cell migration.

Acknowledgments

We thank Dr Dennis Thiele (Duke University, Durham, NC) for the generous gift of $CTR1^{-/-}$ and $CTR1^{+/+}$ mouse embryonic fibroblasts.

Sources of Funding

This work was supported by NIH grants R01 HL070187 (T.F.), R01 HL077524 (to M.U.-F.), and R01 HL080569-01 (to Y.H.); American Heart Association Postdoctoral Fellowship 09POST2250151 (to N.U.); Ruth L. Kirschstein-National Service Research Award (Kirschstein-NRSA) T32 training grant (to G-F.C.); the Uehara Memorial Foundation (to J.O.); the Naito Foundation (to J.O.); American Diabetes Association Research Award 1-10-BS-76 (to Y.H.); and American Heart Association Grant 10GRNT4400005 (to Y.H.). Use of the Advanced Photon Source at Argonne National Laboratory was supported by the US Department of Energy, Office of Science, Office of Basic Energy Sciences, under contract no. DE-AC02-06CH11357.

Disclosures

None.

References

1. Kim BE, Nevitt T, Thiele DJ. Mechanisms for copper acquisition, distribution and regulation. *Nat Chem Biol.* 2008;4:176–185.
2. Schlief ML, Gitlin JD. Copper homeostasis in the CNS: a novel link between the NMDA receptor and copper homeostasis in the hippocampus. *Mol Neurobiol.* 2006;33:81–90.
3. Brewer GJ. Anticopper therapy against cancer and diseases of inflammation and fibrosis. *Drug Discov Today.* 2005;10:1103–1109.
4. Brewer GJ. Iron and copper toxicity in diseases of aging, particularly atherosclerosis and Alzheimer's disease. *Exp Biol Med (Maywood).* 2007; 232:323–335.
5. Ferns GA, Lamb DJ, Taylor A. The possible role of copper ions in atherogenesis: the Blue Janus. *Atherosclerosis.* 1997;133:139–152.
6. Saari JT, Schuschke DA. Cardiovascular effects of dietary copper deficiency. *Biofactors.* 1999;10:359–375.
7. Klevay LM. Cardiovascular disease from copper deficiency–a history. *J Nutr.* 2000;130:489S–492S.
8. Harris ED. A requirement for copper in angiogenesis. *Nutr Rev.* 2004; 62:60–64.
9. Stadler N, Lindner RA, Davies MJ. Direct detection and quantification of transition metal ions in human atherosclerotic plaques: evidence for the presence of elevated levels of iron and copper. *Arterioscler Thromb Vasc Biol.* 2004;24:949–954.
10. Volker W, Dorszewski A, Unruh V, Robenek H, Breithardt G, Buddecke E. Copper-induced inflammatory reactions of rat carotid arteries mimic restenosis/arteriosclerosis-like neointima formation. *Atherosclerosis.* 1997;130:29–36.
11. Mandinov L, Mandinova A, Kyurkchiev S, Kyurkchiev D, Kehayov I, Kolev V, Soldi R, Bagala C, de Muinck ED, Lindner V, Post MJ, Simons M, Bellum S, Prudovsky I, Maciag T. Copper chelation represses the vascular response to injury. *Proc Natl Acad Sci U S A.* 2003;100: 6700–6705.
12. Raines EW. PDGF and cardiovascular disease. *Cytokine Growth Factor Rev.* 2004;15:237–254.
13. Ronnstrand L, Heldin CH. Mechanisms of platelet-derived growth factor-induced chemotaxis. *Int J Cancer.* 2001;91:757–762.
14. Rae TD, Schmidt PJ, Pufahl RA, Culotta VC, O'Halloran TV. Undetectable intracellular free copper: the requirement of a copper chaperone for superoxide dismutase. *Science.* 1999;284:805–808.
15. Kaplan JH, Lutsenko S. Copper transport in mammalian cells: special care for a metal with special needs. *J Biol Chem.* 2009;284:25461–25465.
16. La Fontaine S, Mercer JF. Trafficking of the copper-ATPases, ATP7A and ATP7B: role in copper homeostasis. *Arch Biochem Biophys.* 2007; 463:149–167.
17. Lutsenko S, Barnes NL, Bartee MY, Dmitriev OY. Function and regulation of human copper-transporting ATPases. *Physiol Rev.* 2007;87: 1011–1046.
18. Petris MJ, Voskoboinik I, Cater M, Smith K, Kim BE, Llanos RM, Strausak D, Camakaris J, Mercer JF. Copper-regulated trafficking of the Menkes disease copper ATPase is associated with formation of a phosphorylated catalytic intermediate. *J Biol Chem.* 2002;277:46736–46742.
19. Strausak D, La Fontaine S, Hill J, Firth SD, Lockhart PJ, Mercer JF. The role of GMXCXXC metal binding sites in the copper-induced redistribution of the Menkes protein. *J Biol Chem.* 1999;274:11170–11177.
20. Mercer JF. The molecular basis of copper-transport diseases. *Trends Mol Med.* 2001;7:64–69.
21. Qin Z, Gongora MC, Ozumi K, Itoh S, Akram K, Ushio-Fukai M, Harrison DG, Fukai T. Role of Menkes ATPase in angiotensin II-induced hypertension: a key modulator for extracellular superoxide dismutase function. *Hypertension.* 2008;52:945–951.
22. Payne SL, Hendrix MJ, Kirschmann DA. Paradoxical roles for lysyl oxidases in cancer–a prospect. *J Cell Biochem.* 2007;101:1338–1354.
23. Hurtado PA, Vora S, Sume SS, Yang D, St Hilaire C, Guo Y, Palamakumbura AH, Schreiber BM, Ravid K, Trackman PC. Lysyl oxidase propeptide inhibits smooth muscle cell signaling and proliferation. *Biochem Biophys Res Commun.* 2008;366:156–161.
24. Lucero HA, Ravid K, Grimsby JL, Rich CB, DiCamillo SJ, Maki JM, Myllyharju J, Kagan HM. Lysyl oxidase oxidizes cell membrane proteins and enhances the chemotactic response of vascular smooth muscle cells. *J Biol Chem.* 2008;283:24103–24117.
25. Zhao Y, Min C, Vora SR, Trackman PC, Sonenshein GE, Kirsch KH. The lysyl oxidase pro-peptide attenuates fibronectin-mediated activation of focal adhesion kinase and p130Cas in breast cancer cells. *J Biol Chem.* 2009;284:1385–1393.
26. Jeney V, Itoh S, Wendt M, Gradek Q, Ushio-Fukai M, Harrison DG, Fukai T. Role of antioxidant-1 in extracellular superoxide dismutase function and expression. *Circ Res.* 2005;96:723–729.
27. Wang H, Zhang W, Tang R, Hebbel RP, Kowalska MA, Zhang C, Marth JD, Fukuda M, Zhu C, Huo Y. Core2 1-6-N-glucosaminyltransferase-I deficiency protects injured arteries from neointima formation in ApoE-deficient mice. *Arterioscler Thromb Vasc Biol.* 2009;29:1053–1059.
28. Finney L, Mandava S, Ursos L, Zhang W, Rodi D, Vogt S, Legnini D, Maser J, Ikpatt F, Olopade OI, Glesne D. X-ray fluorescence microscopy reveals large-scale relocalization and extracellular translocation of cellular copper during angiogenesis. *Proc Natl Acad Sci U S A.* 2007; 104:2247–2252.
29. Lin SJ, Pufahl RA, Dancis A, O'Halloran TV, Culotta VC. A role for the Saccharomyces cerevisiae ATX1 gene in copper trafficking and iron transport. *J Biol Chem.* 1997;272:9215–9220.
30. Lee J, Petris MJ, Thiele DJ. Characterization of mouse embryonic cells deficient in the ctr1 high affinity copper transporter. Identification of a Ctr1-independent copper transport system. *J Biol Chem.* 2002;277: 40253–40259.
31. Ridley AJ. Rho GTPases and cell migration. *J Cell Sci.* 2001;114: 2713–2722.
32. Song KS, Li S, Okamoto T, Quilliam LA, Sargiacomo M, Lisanti MP. Co-purification and direct interaction of Ras with caveolin, an integral membrane protein of caveolae microdomains. Detergent-free purification of caveolae microdomains. *J Biol Chem.* 1996;271:9690–9697.
33. Smart EJ, Ying YS, Mineo C, Anderson RG. A detergent-free method for purifying caveolae membrane from tissue culture cells. *Proc Natl Acad Sci U S A.* 1995;92:10104–10108.
34. Maryon EB, Molloy SA, Kaplan JH. O-linked glycosylation at threonine 27 protects the copper transporter hCTR1 from proteolytic cleavage in mammalian cells. *J Biol Chem.* 2007;282:20376–20387.
35. Manes S, Ana Lacalle R, Gomez-Mouton C, Martinez AC. From rafts to crafts: membrane asymmetry in moving cells. *Trends Immunol.* 2003;24: 320–326.
36. Peltonen L, Kuivaniemi H, Palotie A, Horn N, Kaitila I, Kivirikko KI. Alterations in copper and collagen metabolism in the Menkes syndrome and a new subtype of the Ehlers-Danlos syndrome. *Biochemistry.* 1983; 22:6156–6163.
37. Lindner V, Fingerle J, Reidy MA. Mouse model of arterial injury. *Circ Res.* 1993;73:792–796.
38. White C, Kambe T, Fulcher YG, Sachdev SW, Bush AI, Fritsche K, Lee J, Quinn TP, Petris MJ. Copper transport into the secretory pathway is regulated by oxygen in macrophages. *J Cell Sci.* 2009;122:1315–1321.
39. White C, Lee J, Kambe T, Fritsche K, Petris MJ. A role for the ATP7A copper-transporting ATPase in macrophage bactericidal activity. *J Biol Chem.* 2009;284:33949–33956.
40. Veldhuis NA, Valova VA, Gaeth AP, Palstra N, Hannan KM, Michell BJ, Kelly LE, Jennings I, Kemp BE, Pearson RB, Robinson PJ, Camakaris J. Phosphorylation regulates copper-responsive trafficking of the Menkes

copper transporting P-type ATPase. *Int J Biochem Cell Biol.* 2009;41:2403–2412.
41. Cobbold C, Coventry J, Ponnambalam S, Monaco AP. Actin and microtubule regulation of trans-Golgi network architecture, and copper-dependent protein transport to the cell surface. *Mol Membr Biol.* 2004;21:59–66.
42. Pase L, Voskoboinik I, Greenough M, Camakaris J. Copper stimulates trafficking of a distinct pool of the Menkes copper ATPase (ATP7A) to the plasma membrane and diverts it into a rapid recycling pool. *Biochem J.* 2004;378:1031–1037.
43. Hung YH, Robb EL, Volitakis I, Ho M, Evin G, Li QX, Culvenor JG, Masters CL, Cherny RA, Bush AI. Paradoxical condensation of copper with elevated beta-amyloid in lipid rafts under cellular copper deficiency conditions: implications for Alzheimer disease. *J Biol Chem.* 2009;284:21899–21907.
44. Setty SR, Tenza D, Sviderskaya EV, Bennett DC, Raposo G, Marks MS. Cell-specific ATP7A transport sustains copper-dependent tyrosinase activity in melanosomes. *Nature.* 2008;454:1142–1146.
45. Brasselet C, Durand E, Addad F, Al Haj Zen A, Smeets MB, Laurent-Maquin D, Bouthors S, Bellon G, de Kleijn D, Godeau G, Garnotel R, Gogly B, Lafont A. Collagen and elastin cross-linking: a mechanism of constrictive remodeling after arterial injury. *Am J Physiol Heart Circ Physiol.* 2005;289:H2228–H2233.
46. Mercer JF. Menkes syndrome and animal models. *Am J Clin Nutr.* 1998;67:1022S–1028S.

Novelty and Significance

What Is Known?

- Copper is an essential micronutrient in all living organisms and involved in physiological repair processes, as well as various pathophysiologies including atherosclerosis.
- Copper deficiency therapies prevent neointimal thickening in response to vascular injury.
- Platelet-derived growth factor (PDGF) stimulates vascular smooth muscle cell (VSMC) migration, which promotes neointimal formation and vascular remodeling after vascular injury.

What New Information Does This Article Contribute?

- Copper transporter ATP7A plays an important role in PDGF-induced VSMC migration in a copper-dependent manner.
- PDGF stimulation promotes ATP7A translocation from the *trans*-Golgi network (TGN) to the lipid raft microdomains which localize at the leading edge, thereby promoting lamellipodia formation through recruiting Rac1 as well as increasing lysyl oxidase (LOX) activity.
- In vivo, ATP7A expression is upregulated and copper accumulation is observed in neointimal VSMC in response to vascular injury.

Copper, an essential micronutrient, has been implicated in vascular remodeling in response to injury by unknown mechanisms. Because excess copper is toxic, bioavailability of copper is tightly controlled not only by the copper importer CTR1, but also by the copper exporter ATP7A. Function of ATP7A is achieved through copper-dependent translocation from TGN. We investigated a role of ATP7A in PDGF-induced VSMC migration, a key component of neointimal formation after vascular injury. Here we show that depletion of ATP7A inhibits PDGF-induced VSMC migration in a copper/CTR1 dependent manner. Mechanistically, PDGF stimulation promotes ATP7A translocation from TGN to the lipid raft microdomains which localize at the leading edge in migrating VSMCs, thereby promoting lamellipodia formation through recruiting Rac1, as well as regulating LOX activity. In vivo, ATP7A is markedly increased in neointimal VSMC in wire injury model, in which copper accumulation is observed. Our findings uncover an unexpected role of ATP7A as a regulator of vascular migration in response to injury and provide insight into copper transporters as potential therapeutic targets for vascular remodeling and atherosclerosis. Furthermore, our studies will suggest a novel linkage between copper homeostasis and vascular migration.

OPEN ACCESS Freely available online

PLoS one

IQGAP1 Is Involved in Post-Ischemic Neovascularization by Regulating Angiogenesis and Macrophage Infiltration

Norifumi Urao[1], Masooma Razvi[1], Jin Oshikawa[1], Ronald D. McKinney[1], Rupal Chavda[1], Wadie F. Bahou[3], Tohru Fukai[2], Masuko Ushio-Fukai[1]*

1 Department of Pharmacology, Center for Lung and Vascular Biology, Center for Cardiovascular Research, University of Illinois at Chicago, Chicago, Illinois, United States of America, **2** Departments of Medicine and Pharmacology, Center for Cardiovascular Research, University of Illinois at Chicago, Chicago, Illinois, United States of America, **3** Department of Medicine, State University of New York at Stony Brook, Stony Brook, New York, United States of America

Abstract

Background: Neovascularization is an important repair mechanism in response to ischemic injury and is dependent on inflammation, angiogenesis and reactive oxygen species (ROS). IQGAP1, an actin-binding scaffold protein, is a key regulator for actin cytoskeleton and motility. We previously demonstrated that IQGAP1 mediates vascular endothelial growth factor (VEGF)-induced ROS production and migration of cultured endothelial cells (ECs); however, its role in post-ischemic neovascularization is unknown.

Methodology/Principal Findings: Ischemia was induced by left femoral artery ligation, which resulted in increased IQGAP1 expression in $Mac3^+$ macrophages and $CD31^+$ capillary-like ECs in ischemic legs. Mice lacking IQGAP1 exhibited a significant reduction in the post-ischemic neovascularization as evaluated by laser Doppler blood flow, capillary density and α-actin positive arterioles. Furthermore, $IQGAP1^{-/-}$ mice showed a decrease in macrophage infiltration and ROS production in ischemic muscles, leading to impaired muscle regeneration and increased necrosis and fibrosis. The numbers of bone marrow (BM)-derived cells in the peripheral blood were not affected in these knockout mice. BM transplantation revealed that IQGAP1 expressed in both BM-derived cells and tissue resident cells, such as ECs, is required for post-ischemic neovascularization. Moreover, thioglycollate-induced peritoneal macrophage recruitment and ROS production were inhibited in $IQGAP1^{-/-}$ mice. *In vitro*, $IQGAP1^{-/-}$ BM-derived macrophages showed inhibition of migration and adhesion capacity, which may explain the defective macrophage recruitment into the ischemic tissue in $IQGAP1^{-/-}$ mice.

Conclusions/Significance: IQGAP1 plays a key role in post-ischemic neovascularization by regulating, not only, ECs-mediated angiogenesis but also macrophage infiltration as well as ROS production. Thus, IQGAP1 is a potential therapeutic target for inflammation- and angiogenesis-dependent ischemic cardiovascular diseases.

Citation: Urao N, Razvi M, Oshikawa J, McKinney RD, Chavda R, et al. (2010) IQGAP1 Is Involved in Post-Ischemic Neovascularization by Regulating Angiogenesis and Macrophage Infiltration. PLoS ONE 5(10): e13440. doi:10.1371/journal.pone.0013440

Editor: Pieter H. Reitsma, Leiden University Medical Center, Netherlands

Received July 17, 2010; **Accepted** September 24, 2010; **Published** October 15, 2010

Funding: This research was supported by National Institutes of Health (NIH) R01 Heart and Lung (HL)077524 and HL077524-S1 (to M.U.-F.), HL070187 (to T.F.), American Heart Association (AHA) Grant-In-Aid 0755805Z (to M.U.-F.) and AHA National Center Research Program (NCRP) Innovative Research Grant 0970336N (to M.U.-F), AHA Post-doctoral Fellowship 09POST2250151 (to N.U.), Uehara Memorial Foundation and Naito Foundation (to J.O.). The funders had no role in study design, data collection and analysis, decision to publish, or preparation of the manuscript.

Competing Interests: The authors have declared that no competing interests exist.

* E-mail: mfukai@uic.edu

Introduction

Neovascularization in response to ischemia is an important repair process, which is dependent on inflammation and angiogenesis, defined as the process of new vessel formation from pre-existing capillary-like endothelial cells (ECs) as well as arteriogenesis [1]. Macrophage infiltration into ischemic tissues plays a key role in ischemia-induced neovascularization by releasing angiogenic cytokines including vascular endothelial growth factor (VEGF) [1,2,3,4]. They also protect tissues from necrosis, and promote healing/regeneration of muscles during limb ischemia [3,5,6,7]. VEGF induces angiogenesis by stimulating EC migration and proliferation primarily through the VEGF type2 receptor (VEGFR2) [8], as well as by upregulating stromal derived factor-1α (SDF-1α) in ischemic sites, thereby recruiting proangiogenic myeloid cells [9]. Impaired migratory response of bone marrow (BM)-derived cells contributes to inhibition of neovascularization capacity of those cells [10]. We previously reported that reactive oxygen species (ROS) derived from NADPH oxidase expressed in inflammatory cells and ECs play a critical role in ischemia-induced neovascularization [11]. Thus, identifying critical regulators for macrophage-mediated inflammatory responses and angiogenesis is important for understanding the mechanisms of post-ischemic neovascularization and treatment of ischemic heart and limb diseases.

IQ-domain GTPase-activating protein 1 (IQGAP1) is a scaffold protein that plays a pivotal role in regulating actin cytoskeleton and cell migration by interacting directly with actin, active Rac1/

Cdc42, Arp2/3 and N-WASP [12,13,14]. In actively migrating cells, IQGAP1 accumulates at the leading edge and cross-links actin filaments [15,16]. IQGAP1 also binds to actin filament nucleator, Diaphanous-related formin (Dia1), and thus localizing Dia1 at the actin-rich phagocytic cup, which is required for migration and phagocytosis of RAW macrophage [17]. We previously demonstrated that IQGAP1 directly binds to VEGFR2 [18] and it plays a critical role in transmitting VEGF-mediated signals to the angiogenesis-related responses in ECs [18,19]. We have shown that IQGAP1 translocates to the leading edge where it binds to VEGFR2 and NADPH oxidase2, a major source of ROS in ECs, thereby promoting ROS production and directional EC migration [18,20]. Moreover, we found that IQGAP1 expression is dramatically increased in the regenerating ECs layers after vascular injury [18] as well as in capillary-like ECs during angiogenesis after hindlimb ischemia [21]. Meyer et al. recently showed that knockdown of IQGAP1 expression with siRNA inhibits VEGF-induced angiogenesis in an *in vivo* model of chicken chorioallntoic membrane [19]. IQGAP1 has been implicated in cancer and tumorigenesis [22]. However, the role of IQGAP1 in post-ischemic neovascularization remains unknown.

In the present study, we demonstrate that IQGAP1 expression is increased in infiltrated macrophages and ECs in ischemic tissues. Mice lacking IQGAP1 show reduced limb blood flow recovery, capillary density and α-actin positive arterioles, as well as tissue repair. These are due to decreased macrophage infiltration and ROS production in ischemic muscles in IQGAP1$^{-/-}$ mice. Moreover, thioglycollate-induced peritoneal leukocyte recruitment and its ROS production are significantly inhibited in IQGAP1$^{-/-}$ mice. BM reconstitution experiments show that IQGAP1 in both inflammatory cells and ECs are necessary to increase blood flow recovery, capillary density and α-actin positive vessels. *In vitro*, IQGAP1$^{-/-}$ BM-derived macrophages show inhibition of migration due to impaired actin polarization as well as adhesion capacity to fibronectin and vitronectin. Thus, endogenous IQGAP1 plays an important role in ischemia-induced revascularization by regulating macrophage infiltration and EC-mediated angiogenesis.

Methods

Ethics Statement for Animal Study

Study protocols were approved by the Animal Care and Institutional Biosafety Committee of University of Illinois at Chicago (ACC: 09-066).

Animals

IQGAP1$^{-/-}$ mice on mix background [23] were backcrossed with C57BL/6 mice 10 generations. Age matched C57BL6 mice used for control, wild type (WT) mice, were purchased from Jackson Laboratory. All mice were maintained at the University of Illinois at Chicago animal facilities. Mice at 8 to 12 weeks old were used for experiments.

Hindlimb ischemia model

Mice were subjected to unilateral hindlimb surgery under anesthesia with intraperitoneal administration of ketamine (100 mg/kg) and xylazine (10 mg/kg). We performed ligation and segmental resection of left femoral vessels followed by physiological and histological analysis as described [24]. Briefly, the left femoral artery was exposed, ligated both proximally and distally using 6-0 silk sutures and the vessels between the ligatures was excised without damaging the femoral nerve. All arterial branches between the ligations were obliterated using an electrical coagulator (Fine Scientific Tools). Skin closure was done using 6-0 nylon sutures. We measured ischemic (left)/nonischemic (right) limb blood flow ratio using a laser Doppler blood flow (LDBF) analyzer (PeriScan PIM 3 System; Perimed) as we described [25]. Mice were anesthetized and placed on a heating plate at 37°C for 10 minutes to minimize temperature variation. Before and after surgery, LDBF analysis was performed in the plantar sole. Blood flow was displayed as changes in the laser frequency, represented by different color pixels, and mean LDBF values were expressed as the ratio of ischemic to nonischemic LDBF. The incidence and severity of hind limb tissue necrosis was assessed after surgery at indicated time point, severity of necrosis was assessed using the following scale: 0 = no necrosis, 1 = one toe, 2 = two or more toes, 3 = foot necrosis, 4 = leg necrosis, and 5 = autoamputation of the entire leg as described [26].

Histological analysis

For cryosections, mice were euthanized and perfused through the left ventricle with saline and 4% paraformaldehyde, limbs were fixed in 4% paraformaldehyde (PFA) overnight and incubated with 30% sucrose, and adductor and gastrocunemius muscles were embedded in OCT compound (Sakura Finetek). For paraffin sections, we performed methanol fixation or PFA fixation with decalcification by Immunocal (Decal Chemical Corp.). Capillary density in the ischemic muscles was determined in 5 μm cryosections or methanol fixed paraffin sections that were stained with anti-mouse CD31 antibody (BD). Arterioles were stained with Cy3-conjugated anti-αSMA antibody (1A4, Sigma), or anti-αSMA antibody (ASM-1, American Research Products) followed by biotinylated anti-mouse IgG antibody (Vector Laboratories). Monocytes/macrophages were labeled with anti-Mac3 antibody followed by biotinylated anti-rat IgG (Vector Laboratories). For immunohistochemistry, we used R.T.U. Vectorstain Elite (Vector Laboratories) followed by DAB visualization (Vector Laboratories). Images were captured by Axio scope microscope (Zeiss) or confocal microscopy (Zeiss) and processed by AxioVision 4.8 or LSM510 software (Zeiss), respectively.

Thioglycollate-induced peritonitis

Mice were intraperitoneally injected with 1 ml of 4% thioglycollate broth (Sigma). Four days after the injection, mice were killed by CO_2 inhalation. Cells in peritoneal cavity were recovered by peritoneal lavage by injecting intraperitoneally with 3 changes of 3 ml of PBS containing 0.1% BSA, 0.5 mM EDTA and 10 U/ml of heparin as described previously [27]. Total cell and macrophage count were determined by Neubauer hemocytometer under microscopy.

Lucigenin-based $O_2^{\bullet-}$ measurement

Lucigenin-enhanced chemiluminescence assay was performed to measure $O_2^{\bullet-}$ production, as we described [11,25]. Freshly excised adductor muscles or harvested peritoneal cells (1 million cells) were placed in scintillation vials containing Krebs-HEPES buffer with 5 μM lucigenin. Light emission was detected with a scintillation counter programmed in out-of-coincidence mode. The mean chemiluminescence yields observed during a period of 30 minutes after addition of the samples were used to estimate rates of production of $O2^{\bullet-}$.

$O_2^{\bullet-}$ detection in mice

Dihydroethidium (Invitrogen) was prepared as a 1 mg/ml solution in 1% DMSO and administered at 1 mg per kg of body weight by intraperitoneal injection as reported previously[28].

Mice were killed and perfusion-fixed with 4% paraformaldehyde 30 minutes after DHE injections. Frozen sections of ischemic muscles were prepared and observed with confocal microscope (Zeiss) with excitation at 510–550 nm and emission >585 dsx7Anm to detect oxidized ethidium.

Isolation and primary culture of bone marrow (BM)-derived macrophages

Bone marrow (BM) mononuclear cells (BMCs) were harvested from tibiae and femurs of 8 to 12 week-old IQGAP1$^{-/-}$ and WT mice as we described previously [25]. Briefly, the BMCs were flushed from the bone with a 27G needle connected to a syringe filled with DPBS with penicillin/streptomycin and 2% FBS. Following density gradient separation by Histopaque 1077 (Sigma), the cells were cultured in DMEM medium (Gibco) supplemented with antibiotics, 10% FBS and 10 ng/ml M-CSF-1 (Peprotech). Non-adherent cells were collected after 24 hours, seeded on coverslips and differentiated for 7 days in polystyrene culture plates. The resulting BM-derived macrophages (BMMs) population was determined by staining with anti-CD11b (BD) and anti-F4/80 (BioLegend) as assessed by flow cytometry (DAKO) as described previously [29,30].

Western blotting- Western blotting was performed as described previously [31]. Briefly, excised adductor muscles and isolated BMCs obtained from IQGAP1$^{-/-}$ and WT mice at 0, 3 and 7 days after hindlimb ischemia were homogenized, and lysates were used for Western blotting analysis with primary antibodies.

BM transplantation

BMCs were isolated by density gradient separation. Recipient mice were lethally irradiated with 9.5 Gy and received an intravenous injection of 3 million donor bone marrow cells 24 hours after irradiation. To determine the transplantation efficiency, transplantation was performed between CD45.1 mice (Jackson Laboratories) and ether IQGAP1 KO or WT mice and peripheral white blood cells were stained with anti-CD45.1 (BD) and anti-CD45.2 (BD). Hindlimb ischemia was induced 6 to 8 weeks after bone marrow transplantation.

Cell migration assays

Migration assays were performed in a modified Boyden chamber, as described previously [25]. Briefly, BMMs were starved in M-CSF-1 overnight and serum for 4 hours before detaching and collecting by scraping. The lower chamber was filled with SDF-1α (PeproTech, 100 μg/ml) in RPMI, the upper chamber with monocytes/macrophage (0.5×10^6/ml). Cells migrated for 4 hours in the presence or absence of SDF-1α. Cells were quantified under the microscope by blinded investigators. Two separate experiments were performed.

Immunostaining in BMMs

BMMs were obtained as described above. After serum and M-CSF-1 starvation at 37°C for 4 hour, SDF-1α (100 ng/ml) or PBS were added and incubated for 2 minutes. After fixation with 2% paraformaldehyde, permeablization by 0.05% tritonX-100 solution and blocking in 3% BSA for 1 hour at room temperature, cells were stained by Alexa-568 conjugated anti-phalloidin (Invitrogen) and anti-IQGAP1 (Santa Cruz). For IQGAP1, primary antibody was labeled with TRITC conjugated anti-rabbit IgG (Jackson Immuno Research). Images were taken by confocal microscopy (Zeiss).

Flow cytometory (FACS) analysis

Peripheral blood was collected in heparinized hematocrit capillary tubes (Fisher scientific) and placed in 150 μl 2% Dextran T500 in PBS plus 150 μl 3 mg/ml EDTA in PBS with 1 unit/ml heparin. The peripheral blood was allowed to settle for 30 min at room temperature. Then the top phase was collected and spun down at 500 *g* for 5 min at 4°C. The supernatant was discarded and the cells were resuspended in 1 ml of RBC lysis buffer (9 ml 0.16 M NH_4Cl +1 ml 0.17 M Tris-Cl, pH 7.65) for 10 min at room temperature. Samples were then washed with DPBS/2% FCS and centrifuged at 500 *g* for 5 min at 4°C. Cells were resuspended in cold DPBS/2% FCS and placed on ice. Total leukocytes in the peritoneal cavity were collected as described above. Cells were stained with the appropriate antibodies; Ly-6C, Ly-6G, Flk-1, CXCR4, Sca-1 and CD11b (BD Pharmingen); cKit, Gr-1 and F4/80 (eBioscience); VEGFR1 (R&D systems). The cells were then washed, resuspended in 2 μg/ml propidium iodide in DPBS/2% FCS, and analyzed on a flow cytometer (DAKO ADP Cyan). Summit (DAKO) or FlowJo 7.6 software was used for population analysis.

Isolation of monocytes/macrophages from muscle

Excised tibiaris anterior muscles were dissociated in DPBS containing collagenase B 0.2%(w/v) (Roche Diagnostics) and 20 mM HEPES at 37°C for 1 hour followed by passing through the 18G and the 23G needles, filtered and counted. The cells suspension was stained with specific antibodies and analyzed on a flow cytometer described above.

Quantitative RT-PCR

Total RNA was prepared from cells or tissues using Tri Reagent (Molecular Research Center Inc.). Reverse transcription was carried out using high capacity cDNA reverse transcription kit (Applied biosystems). Quantitative PCR was performed with the ABI Prism 7000, the SYBR Green PCR kt (Qiagen) and the QuantiTect Primer Assay (Quiagen) for specific genes. Expression of genes was normalized and expressed as fold-changes relative to GAPDH.

Cell-matrix Adhesion Assay

Ninety-six-well plates were coated over night at 4°C with 5 μg/ml purified human fibronectin (Sigma), 5 μg/ml human vitronectin (Chemicon International), 10 μg/ml human type IV collagen (Chemicon International), 10 μg/ml human fibrinogen (Enzyme Research Laboratories) or 10 μg/ml soluble recombinant human ICAM-1 (Axxora Platform), and then blocked for 1 hour at room temperature with 0.5% (w/v) heat-inactivated bovine serum albumin (BSA) in PBS. Cultured BMMs were detached from the culture plates with 1 mM EDTA in PBS after serum and M-CSF-1 starvation at 37°C for 4 hour. Cells suspended with PBS (with Ca^{++} and Mg^{++}) were seeded at 2.5×10^5 cells/well in 100 μl in the coated wells for 30 min. Non-adherent cells were removed by washing, and adherent cells were stained by 0.05% crystal violet and quantified in duplicates by light absorbance (562 nm).

Statistical analysis

All the experiments were repeated at least three times, and all values were expressed as means. Blood flow recovery in the ischemic hindlimb was compared between the two groups by two-way repeated measures ANOVA, followed by Bonferroni post hoc analysis. Comparison between groups was analyzed by unpaired Student 2-tailed t test (2 groups) or ANOVA for experiments with more than 2 subgroups followed by Bonferroni post hoc analysis. $P<0.05$ was considered as statistically significant.

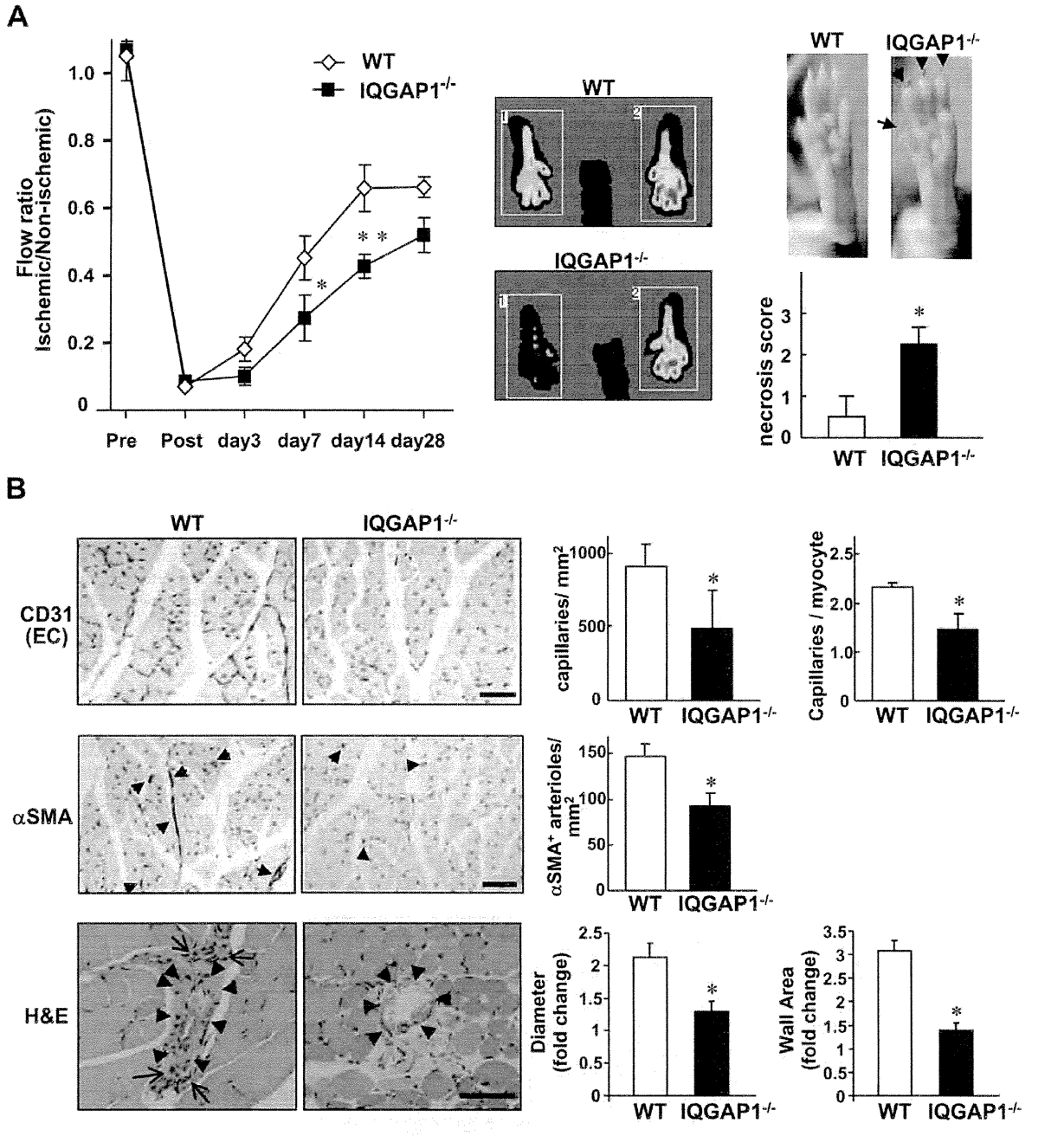

Figure 1. Post-ischemic revascularization is impaired in IQGAP1$^{-/-}$ mice. A, Left, blood flow recovery after hindlimb ischemia in wild-type (WT) and IQGAP1$^{-/-}$ mice, as determined by relative values of laser Doppler perfusion of the plantar sole between ischemic (left) and non-ischemic (right) legs (WT, n = 13; IQGAP1$^{-/-}$, n = 10, **p<0.01 and *p<0.05). Middle panels show representative perfusion images at day 14. Right, tissue necrotic score on the ischemic feet was determined (n = 10 *p<0.05). In IQGAP1$^{-/-}$, the necrotic score represents severe phenotype with edematous fingers and degenerative nail beds (black arrows). **B**, Tissues were harvested at day 14 for histological analysis. CD31 positive capillary-like ECs (top) and α-smooth muscle actin (αSMA) positive arterioles (middle) in ischemic gastrocunemius muscles. Positive staining (red brown) and nuclei (purple) are shown. Bars represent 50 μm. The graphs represent the number per mm in 2 area and/or per muscle fibers (n = 4, *p<0.05). Hematoxyline and eosin (H&E) staining of adductor muscles (bottom). Arrowheads show collateral vessels in semimembranosus muscle. Prominent cellular infiltration in adventitia and perivascular area in WT mice are shown by arrows (left). The diameter and wall area are calculated from the measurements of luminal and perivascular tracing (right). Data shown are mean+/−SEM.
doi:10.1371/journal.pone.0013440.g001

Results

IQGAP1 is involved in Neovascularization in Response to Hindlimb Ischemia

To examine the role of endogenous IQGAP1 in post-ischemic neovascularization, wild-type (WT) and IQGAP1$^{-/-}$ mice were subjected to unilateral hindlimb ischemia. Laser Doppler blood flow (LDBF) analysis showed that the blood flow recovery in ischemic feet at day 7 and 14 was significantly reduced in IQGAP1$^{-/-}$ mice as compared to wild type (WT) mice (left, Figure 1A). Postischemic blood flow recovery in IQGAP1$^{-/-}$ mice gradually caught up to the level of WT mice at day 28, but it was still lower than that in WT mice. In addition, IQGAP1$^{-/-}$ mice increased tissue damage, characterized by toe edema, degeneration on the nail beds and some degree of necrosis measured using a five-point scale (right, Figure 1A). Immunohistochemical analysis revealed that the numbers of CD31-positive capillary-like ECs as well as α-smooth muscle actin-positive arterioles in ischemic tissues at day 7 were significantly decreased in IQGAP1$^{-/-}$ mice (Figure 1B). Histological analysis showed that increase in collateral lumen and wall area in semimembnosus muscle in WT mice [32] were significantly reduced in IQGAP1$^{-/-}$ mice. On day 28, regeneration was widely observed in tibialis anterior muscles in WT mice, which was inhibited in IQGAP1$^{-/-}$ mice that had more necrotic myofibers and large area of fibrosis (Supplemental Figure S1). Thus, IQGAP1 is involved in post-ischemic flow recovery by regulating angiogenesis and arteriogenesis as well as tissue repair and protection from necrosis.

IQGAP1 Expression is increased in Ischemic Muscles after Hindlimb Ischemia

We next examined if the levels of endogenous IQGAP1 are regulated after hindlimb ischemia *in vivo*. Western analysis showed that IQGAP1 protein expression was increased in ischemic muscles at days 3 and 7 after hindlimb ischemia (Figure 2A). Immunofluorescence analysis revealed that IQGAP1 protein expression was highly expressed in Mac-3^{+} macrophages on day 3 and CD31-positive ECs on day 7 in ischemic tissues (Figure 2B). These results suggest that tissue ischemia increases IQGAP1-positive inflammatory cells and ECs, which may contribute to neovascularization.

IQGAP1 is involved in Macrophages Recruitment without affecting Mobilization of Monocytes or Angiogenic Cells after Ischemic Injury

To determine the functional significance of upregulation of IQGAP1 in ischemic tissues, we next examined the role of IQGAP1 in inflammatory cell recruitment into ischemic sites. Figure 3A shows that Mac3^{+} cell recruitment to the ischemic area in the lower limbs (upper) and perivascular area in upper limbs (lower), which contribute to angiogenesis and arteriogenesis/collateral expansion [33], were significantly reduced in IQGAP1$^{-/-}$ mice. Furthermore, we examined M1 and M2 phenotype of macrophages in ischemic muscles and found that the number of both pro-inflammatory macrophages/monocytes and anti-inflammatory macrophages was reduced in IQGAP1$^{-/-}$

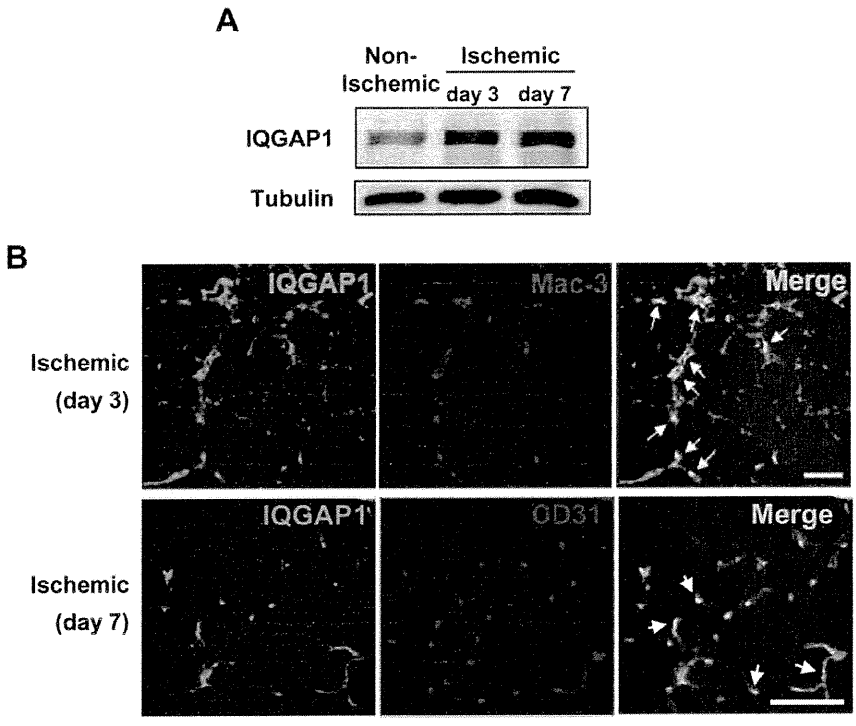

Figure 2. IQGAP1 expression is increased at macrophages and endothelial cells in ischemic hindlimbs. A, Representative Western blots for IQGAP1 or α-tubulin in adductor muscle at day 0, 3, and 7 after hindlimb ischemia. **B**, Representative staining for IQGAP1 (green) or Mac-3, macrophage marker (red) or their colocalization (merge) on day 3, and IQGAP1 (green) or CD31, EC marker (red) or their colocalization (merge) on day 7 in ischemic adductor muscles. Arrows represent colocalization with IQGAP1/Mac-3 or IQGAP1/CD31. Bars represent 100 μm.
doi:10.1371/journal.pone.0013440.g002

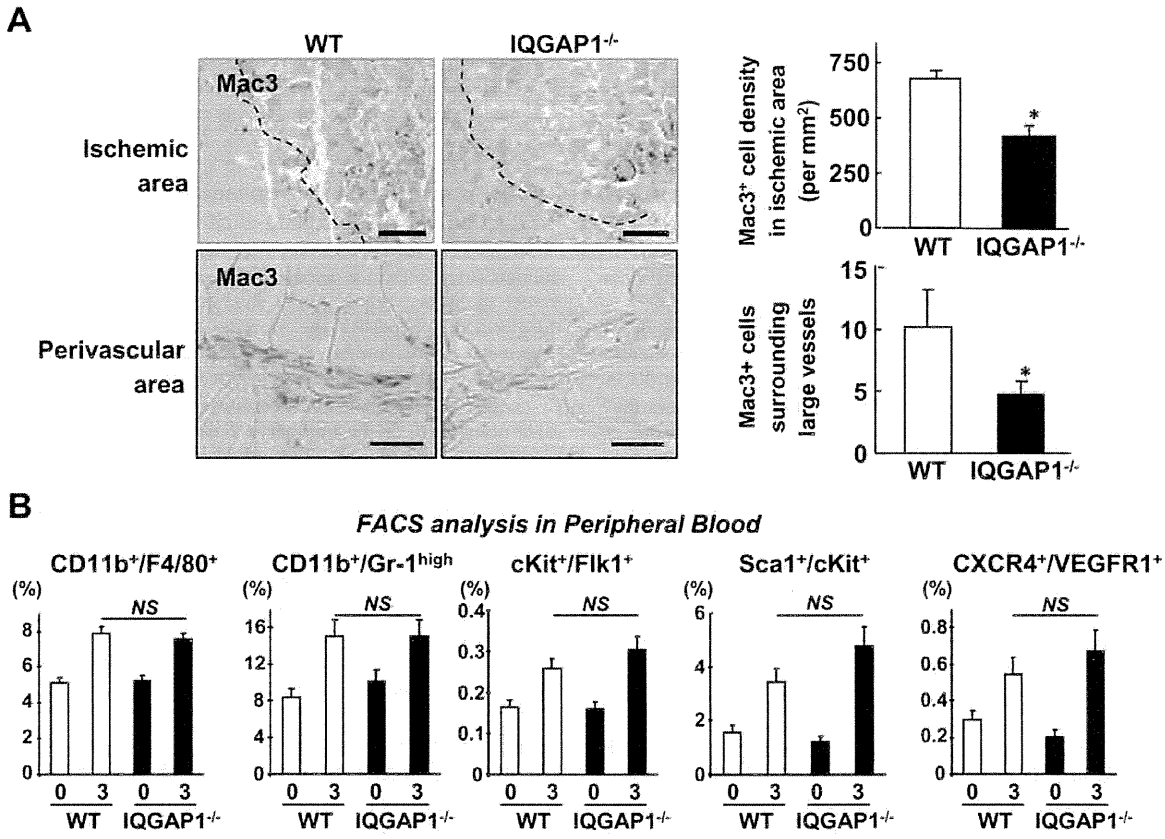

Figure 3. Macrophage infiltration into ischemic muscle, but not its mobilization into circulation, is impaired in IQGAP1$^{-/-}$ mice. A, Immunostaining of Mac3 (monocyte/macrophage marker) in ischemic muscles from WT or IQGAP1$^{-/-}$ mice at day 3. Upper, Mac3 positive cells in ischemic area lacking the original integrity of myofibers on eosin staining (upper left). The border of ischemic area is shown by dotted lines. Bars represent 100 μm. The density of Mac3 positive cells localized in the interstitium were determined (upper right, n = 3, *p<0.05). Lower, Mac3 positive cells in perivascular area of vessels in semimembranosus muscles (lower left). Bars represent 20 μm. The number of Mac3 positive cells distributed in the adventitia and the connective tissue surrounding the large vessels (>50 μm of diameter) were counted (lower right). B, Peripheral blood was obtained at day 0 (no ischemia surgery) and day 3. Total leukocytes were stained by fluorescence-conjugated various antibodies as indicated and analyzed by flow cytometory (n = 3 or 4 in each group). The data is expressed as the percentage of cells in total circulating leukocytes. Data shown are mean+/−SEM.
doi:10.1371/journal.pone.0013440.g003

mice (Supplemental Figure S2A). In addition, expression of both pro-inflammatory cytokine (TNFα) and anti-inflammatory cytokine (IL-10) in ischemic tissues was decreased in IQGAP1$^{-/-}$ mice, which was associated with reduced macrophage number, as measured by colony-stimulating factor receptor (c-fms) expression (Supplemental Figure S2B). These results suggest that

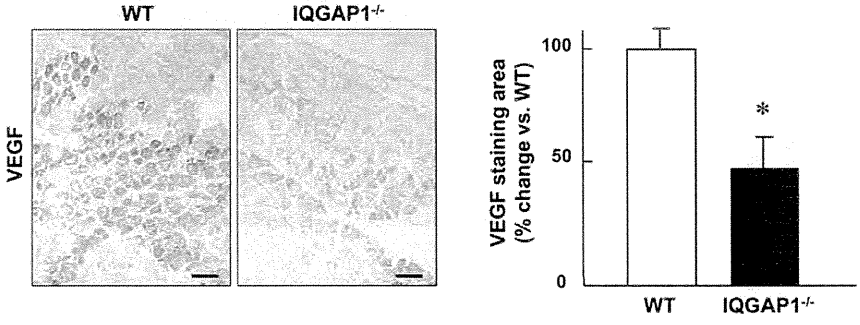

Figure 4. IQGAP1$^{-/-}$ mice show reduced VEGF expression in ischemic muscle. Immunohistochemical staining of VEGF in ischemic adductor muscles at day 3. Brown staining shows VEGF positive cells and counter staining by hematoxylin was performed.
doi:10.1371/journal.pone.0013440.g004

IQGAP1 regulates macrophages infiltration without affecting their polarization capacity. Moreover, the levels of circulating monocytes ($CD11b^+/F4/80^+$ and $CD11b^+/Gr\text{-}1^{high}$) as well as endothelial progenitor cells ($cKit^+/Flk^+$), $Sca1^+/cKit^+$ progenitors or $CXCR4^+VEGFR1^+$ cells in peripheral blood at baseline or after ischemia were not different between WT and $IQGAP1^{-/-}$ mice, as measured by FACS analysis (Figure 3B). We also found that VEGF expression in ischemic tissue was significantly decreased in $IQGAP1^{-/-}$ mice (Figure 4).

IQGAP1 is involved in ROS production after Hindlimb Ischemia

Since IQGAP1 is expressed in both macrophages and capillary-like ECs (Figure 2), which are major sources of ROS in ischemic tissue [11], we next examined the role of IQGAP1 in ROS production induced by hindlimb ischemia. Figure 5A shows that ischemia-induced increase in O_2^- production in ischemic tissue at day 7, as measured by lucigenin chemiluminescence assay, was significantly inhibited in $IQGAP1^{-/-}$ mice. To confirm further this result, we also injected the O_2^- specific dye, dihydroethidium (DHE), into the mice [28] and found that ischemia-induced increase in DHE staining *in situ* was markedly reduced in $IQGAP1^{-/-}$ mice (Figure 5B).

IQGAP1 in both BM-derived and Tissue Resident Cells is required for Ischemia-induced Neovascularization

Since we found that IQGAP1 is highly expressed in both ECs and monocytes/macrophages in ischemic tissue, we next examined the relative role of IQGAP1 in BM-derived cells (BMCs) and tissue resident cells in post-ischemic neovascularization. Western analysis confirmed that IQGAP1 is abundantly expressed in BMCs, which is further upregulated by contra lateral hindlimb ischemia (Figure 6A). We thus performed BM transplantation (BMT) between WT and $IQGAP1^{-/-}$ mice. Reconstitution of WT BM into lethally irradiated $IQGAP1^{-/-}$ mice or $IQGAP1^{-/-}$ BM into irradiated WT mice showed reduction in blood flow recovery (Figure 6B), increased tissue necrosis score (Figure 6C), as well as decreased number of $CD31^+$ capillary like ECs and αSMA^+ arterioles (Figure 6D) as compared to control group (WT mice reconstituted with WT-BM). These results suggest that IQGAP1 expressed in both BM-derived circulating cells and tissue resident cells including ECs contributes to ischemia-induced neovascularization.

IQGAP1 is involved in Macrophage Recruitment and ROS production in Thioglycollate-elicited Peritonitis Model

To address further the role of IQGAP1 in recruitment of inflammatory cells, we used a thioglycollate-elicited peritonitis model to induce non-bacterial inflammation [27]. Injection of thioglycollate increased the number of macrophages in the peritoneal cavity compared with PBS injection in WT mice, which was significantly inhibited in $IQGAP1^{-/-}$ mice (Figure 7A). By contrast, either neutrophil recruitment to the peritoneal cavity (data not shown) or the number of leukocyte in peripheral blood before and after thioglycollate challenge (Figure 7B) was not changed in $IQGAP1^{-/-}$ mice. We also found that O_2^- levels in macrophages obtained from peritoneal cavity were significantly reduced in $IQGAP1^{-/-}$ cells (Figure 7C). Subpopulation analysis for the monocytes/macrophages in the peritoneal cavity showed that there was no significant difference for the pro-inflammatory and anti-inflammatory phenotypes between WT and $IQGAP1^{-/-}$ mice (Supplemental Figure S2C). Thus, IQGAP1 seems to be involved in macrophage recruitment and ROS production without affecting macrophage polarization.

IQGAP1 is involved in Migration and Adhesion of BM-derived Macrophages

To determine the mechanism by which IQGAP1 regulates macrophage recruitment, we examined the role of IQGAP1 in macrophage migration. BMCs isolated from mice were cultured for 7 days in the presence of macrophage colony stimulating factor 1 (MCSF1) to differentiate into monocytes/macrophage as described previously [29]. The differentiation capacity into macrophages was similar between WT- and $IQGAP1^{-/-}$ BMCs,

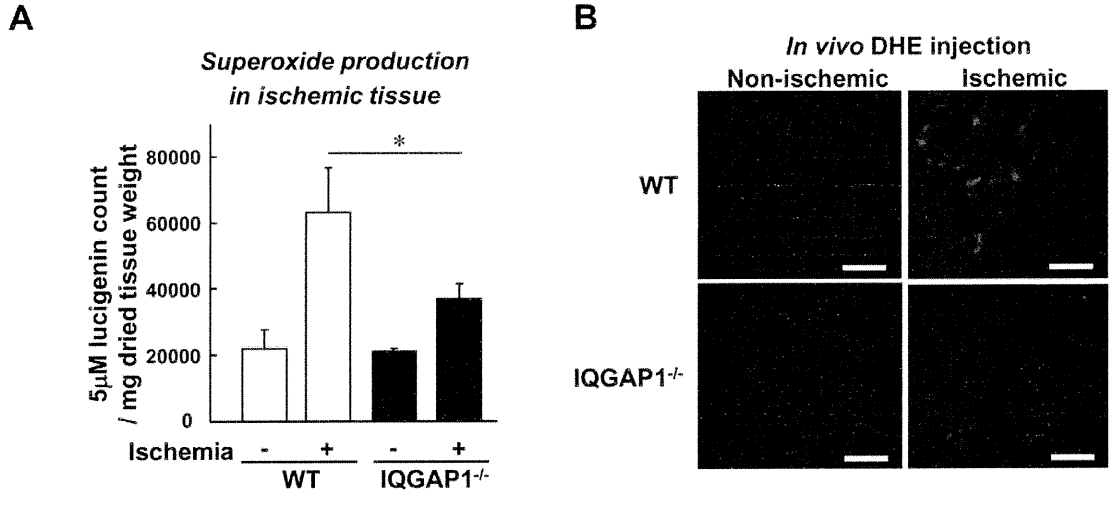

Figure 5. ROS production in ischemic muscles is impaired in $IQGAP1^{-/-}$ mice. A, Superoxide (O_2^-) production was measured in ischemic muscles at day 0 (without surgery) and 7 days after hindlimb ischemia, using lucigenin chemiluminescence. The values were normalized by tissue dry weight ($n=4$, $^*p<0.05$). **B**, O_2^- detection probe, dihydroethidium (DHE) was injected into mice at 30 minutes before sacrifice on day 7 after hindlimb ischemia, and tissues were harvested following perfusion fixation. DHE-positive signals (arrows) in non-ischemic and ischemic muscles of frozen sections (20 μm thickness) were observed with confocal microscope. Bars represent 20 μm.
doi:10.1371/journal.pone.0013440.g005

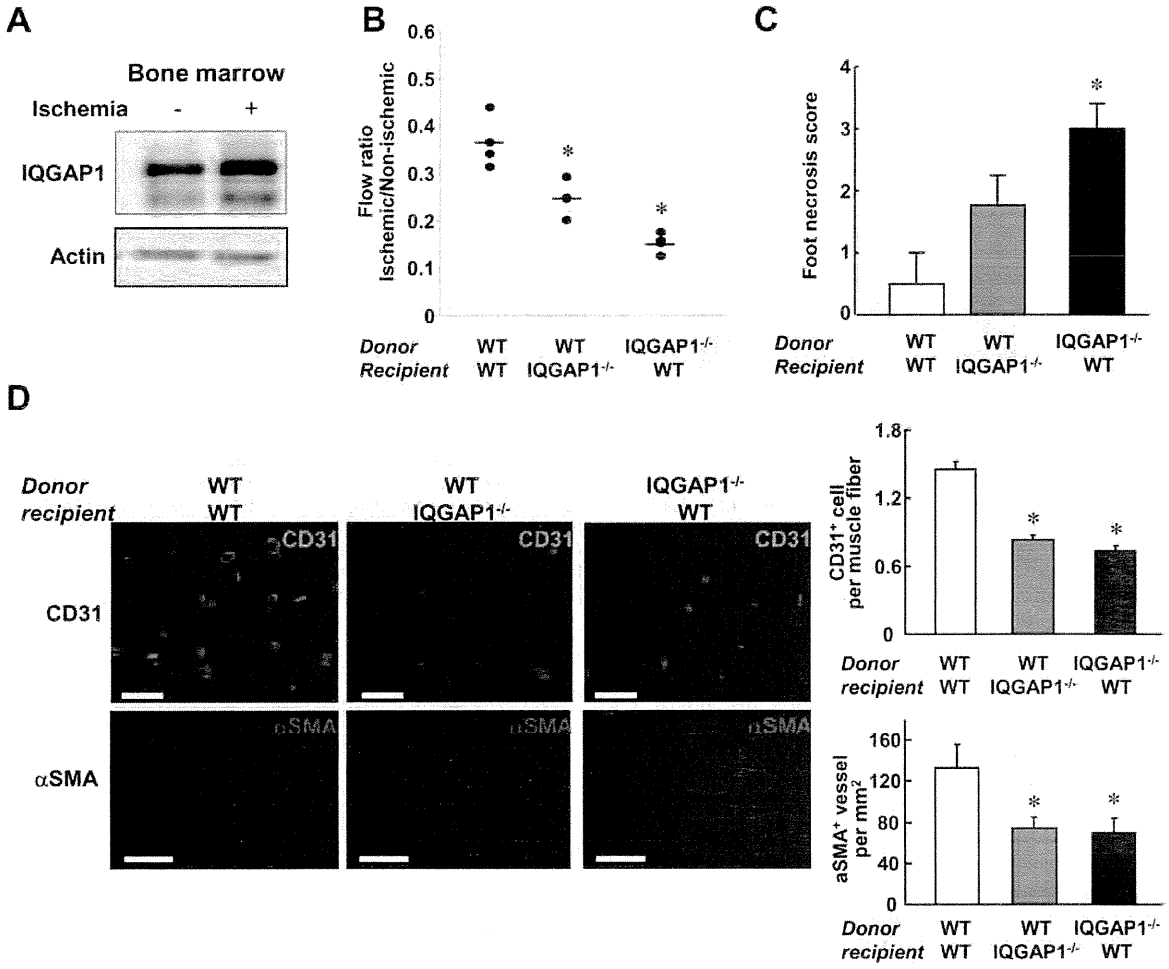

Figure 6. IQGAP1$^{-/-}$ mice show reduced macrophage recruitment and ROS production in thioglycollate-elicited peritonitis model. Macrophage recruitment was induced by intraperitoneal (i.p.) injection of 4% thioglycollate (+) or PBS (−) into WT and IQGAP1$^{-/-}$ mice. **A**, Number of macrophages recruited to the peritoneal cavity at 4 days after thioglycollate injection (n = 4, **p<0.01). **B**, Number of leukocytes in peripheral blood collected from the same animals as shown in A. **C**, O_2^- production in recruited leukocytes at 4 days after injection, as measured by lucigenin chemiluminescence assay (n = 4 total, *p<0.05). The values were normalized by the number of peritoneal macrophages.
doi:10.1371/journal.pone.0013440.g006

as measured by the percentage of CD11b and F4/80 expressions with flow cytometry analysis (Supplemental Figure S3A). However, the morphology of IQGAP1$^{-/-}$ BM-derived macrophages (BMMs) attached on the culture dish or the glass cover slip were rounder compared to WT cells (Supplemental Figure S3B). Modified Boyden chamber assay showed that IQGAP1$^{-/-}$ BMMs had impaired migration in response to chemokine, SDF-1α (Figure 8A), but not to VEGF (Supplemental Figure S4B). Of note, SDF-1α expression in ischemic tissues was not significantly different between WT and IQGAP1$^{-/-}$ mice (data not shown), while VEGF expression was markedly reduced in IQGAP1$^{-/-}$ mice (Figure 4). Thus, endogenous IQGAP1 is involved in SDF-1/CXCR4-mediated migration of BMMs, thereby promoting infiltration of macrophages into the ischemic tissues. Since actin polymerization is an important mechanism for migration, and IQGAP1 is known to directly bind to F-actin, we next examined the role of IQGAP1 in BMMs for this response. Immunofluorescence analysis showed that IQGAP1 was colocalized with F-actin at the plasma membrane in SDF-1α-stimulated BMMs (Figure 8B). SDF-1α-induced actin polarization was markedly inhibited in IQGAP1$^{-/-}$ macrophages (Figure 8B). Thus, IQGAP1 is involved in chemotaxis of BM macrophages at least in part by regulating actin reorganization. Further, we assessed adhesion capacity of BMMs. We found that IQGAP1$^{-/-}$ BMMs had a lower adhesion capacity to fibronectin and vitronectin as compared to WT BMMs (Figure 8C).

Discussion

The present study uncovers a novel role of IQGAP1 in post-ischemic neovascularization and tissue repair by regulating not only angiogenesis but also macrophage infiltration to ischemic tissues. Here we show that: 1) Hindlimb ischemia increases IQGAP1 expression in infiltrating macrophages and ECs in ischemic tissues; 2) Mice lacking IQGAP1 show decreased blood flow recovery, capillary density and α-SMA-positive arterioles, and increased damage in ischemic tissue; 3) Macrophage recruitment and ROS production in ischemic tissue, but not the number of

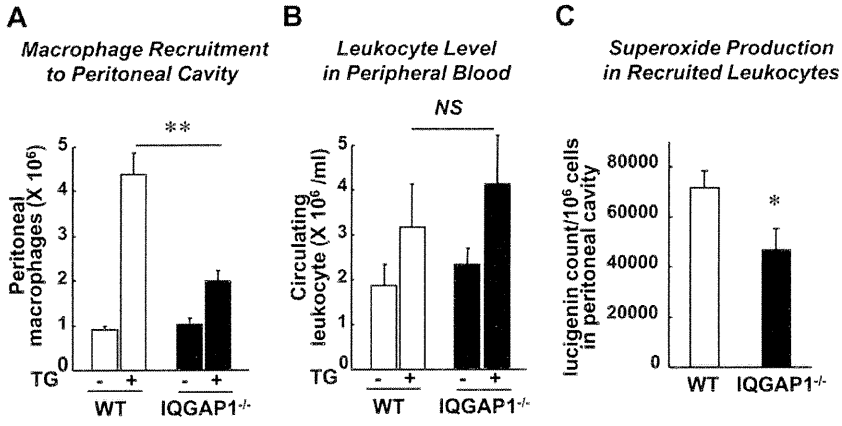

Figure 7. IQGAP1 in both bone marrow-derived and tissue resident cells is required for ischemia-induced neovascularization. A, Western analysis for IQGAP1 protein expression in whole bone marrow lysate (40 μg protein) obtained from femurs of healthy leg in mice subjected to contralateral hindlimb ischemia (day 3). Actin was used as loading control. **B–D,** Bone marrow transplantation (BMT) was performed between WT and IQGAP1$^{-/-}$ mice. After 6 weeks of irradiation, BMT mice were subjected to hindlimb ischemia and observed for 21 days. Blood flow measured at day 21 (n = 4, *p<0.05 vs. WT-WT)(**B**), necrosis score as Figure 1 (n = 4, *p<0.05 vs. WT-WT)(**C**), and representative images of ischemic muscles stained by anti-CD31- (green) or anti-αSMA- (red) antibodies (**D**, left). Bars show 50 μm. In **D** (right), the numbers of CD31 positive ECs per muscle fiber or αSMA positive vessels per mm^2 in ischemic muscles were obtained (n = 4, *p<0.05 vs. WT-WT). Data shown are mean+/−SEM.
doi:10.1371/journal.pone.0013440.g007

circulating monocytes, are significantly inhibited in IQGAP1$^{-/-}$ mice; 4) BM reconstitution experiments show that IQGAP1 in both BM-derived and tissue resident cells contribute to capillary formation and α-SMA positive pericyte recruitment in ischemic tissue; 5) Mechanistically, IQGAP1$^{-/-}$ BM-derived macrophages show an inhibition of migration and adhesion capacity.

Post-ischemic neovascularization is a complex process coordinated by angiogenic ECs and recruited inflammatory cells. We and others have previously demonstrated that IQGAP1 directly binds to VEGFR2 or cSrc and B-Raf, and knockdown of endogenous IQGAP1 with siRNA inhibits VEGF-induced angiogenic responses in cultured ECs [18,19,20]. We also reported that IQGAP1 expression is upregulated in regenerating ECs in response to vascular [18] or ischemic injury [21]. However, a role of endogenous IQGAP1 in ischemia-induced neovascularization was virtually unexplored. Here we provide compelling evidence that ischemia-induced increases in CD31$^+$ capillary-like ECs (angiogenesis) and α-SMA$^+$ arterioles (pericyte recruitment) are significantly reduced in IQGAP1$^{-/-}$ mice, thereby inhibiting blood flow recovery at days 7 and 14 after ischemia. Consistent with our results, Meyer et al. recently reported that depletion of IQGAP1 with siRNA suppresses VEGF-induced angiogenesis in an *in vivo* model of chicken chorioallantoic membrane [19]. In the current study, postischemic blood flow recovery in IQGAP1−/− mice gradually catch up to that of WT mice at day 28 but not to the level seen in WT mice. Together with histological analysis, these results suggest that IQGAP1 plays an important role in post-ischemic neovascularization *in vivo* by regulating arteriogenesis and angiogenesis.

The present study also demonstrates that IQGAP1 expression is increased in ischemic tissues, which may be due to increased, infiltrated macrophages and newly formed ECs, which express IQGAP1, at day 3 and 7, respectively. Functionally, IQGAP1−/− mice show impaired recruitment of monocytes/macrophages into ischemic tissue and perivascular areas in the upper limbs, which is associated with lower expression of VEGF. It has been shown that macrophage-derived VEGF contributes to angiogenesis and arteriogenesis in ischemic tissues [1,2,3,4] and that the recruitment of macrophages participate in arteriogenesis, blood flow recovery, and angiogenesis [34]. Thus, IQGAP1-dependent inflammatory cells recruitment maybe required for post-ischemic neovascularization. The role for IQGAP1 in BM-derived macrophages and ECs in the hindlimb ischemia model is demonstrated by BMT experiments. Transfer of WT-BM to recipient IQGAP1$^{-/-}$ mice or IQGAP1$^{-/-}$ BM to WT recipients lowers blood flow recovery, capillary density and α-SMA$^+$ arterioles in ischemic tissues than WT mice transplanted with WT-BM. These results suggest that IQGAP1 expressed in both BM-derived cells and tissue resident cells, including ECs, plays an important role in reparative neovascularization in response to tissue ischemia. We cannot exclude the possible involvement of IQGAP1 in tissue resident macrophages in this study.

Infiltrated macrophages are also critical to tissue healing and regeneration after ischemic injury [3,5,6,7]. The present study demonstrates that regeneration of skeletal muscle is impaired in association with an increase in necrosis and fibrosis in IQGAP1$^{-/-}$ mice at later phase after hindlimb ischemia, suggesting that IQGAP1 plays an important role in macrophage function. This is consistent with a previous study showing reduced phagocytotic activity of IQGAP1-depleted RAW macrophages *in vitro* [17]. Thus, IQGAP1-mediated inflammatory cell recruitment may contribute to angiogenesis and repair/regeneration of muscle, thereby promoting restoration of perfusion in the ischemic limbs. In this study, we found that the lack of IQGAP1 does not affect mobilization of BM-derived cells including monocytes and other angiogenic cells to peripheral blood after hindlimb ischemia. Similar results were obtained in a non-bacterial inflammation peritonitis model, where thioglycollate-elicited peritoneal macrophage infiltration to tissue is inhibited in IQGAP1$^{-/-}$ mice, with no difference in the level of circulating leukocytes. Furthermore, M1 and M2 phenotype analysis of macrophages in ischemic tissues and peritoneal macrophages reveal that IQGAP1 is seemingly not involved in macrophage polarization. Thus, these results indicate that IQGAP1 is generally involved in macrophage recruitment during inflammation without affecting their mobilization from BM or polarization, which may contribute to neovascularization and tissue repair in response to injury.

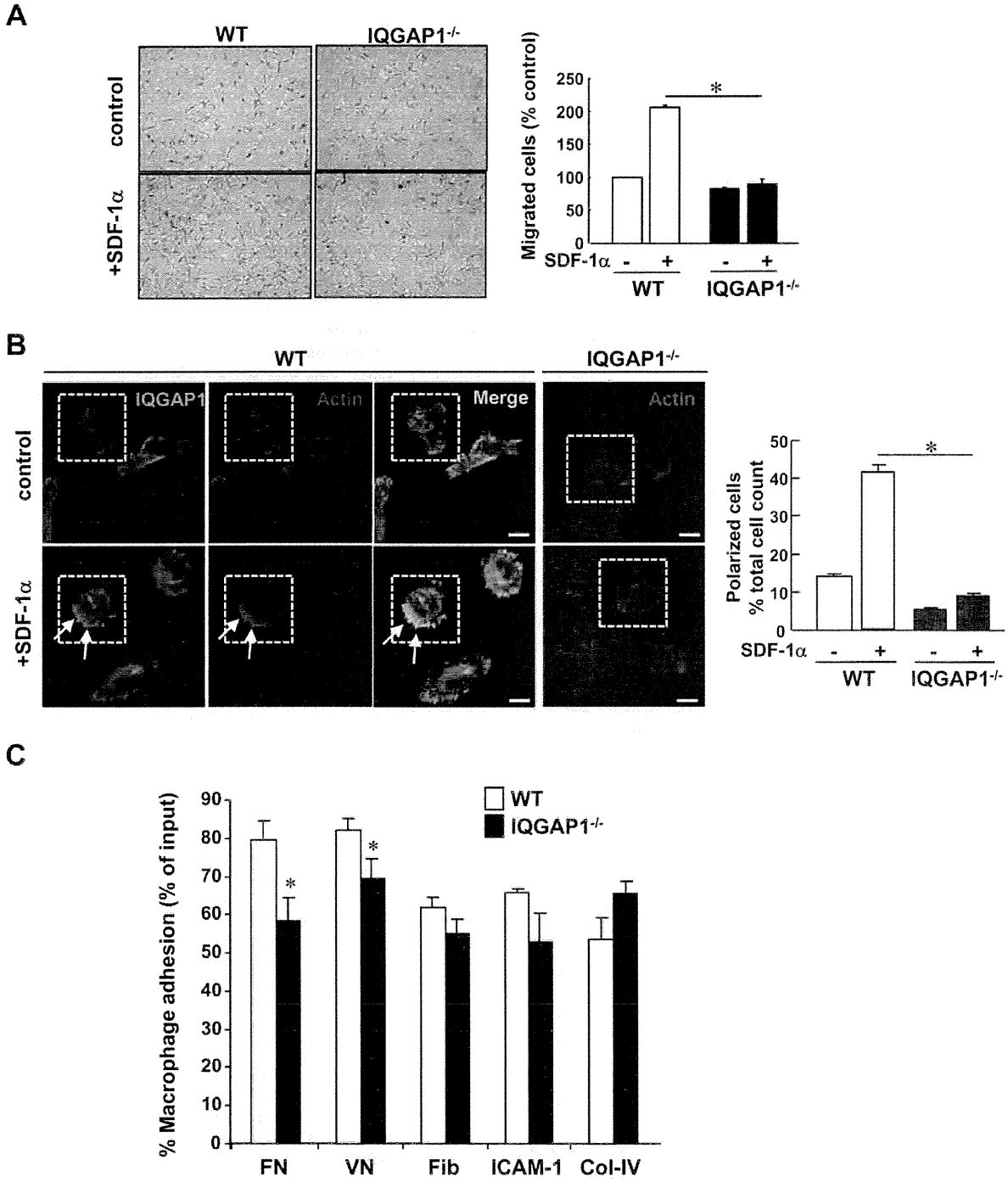

Figure 8. Migration capacity and actin polarization are impaired in IQGAP1$^{-/-}$ BM-derived macrophages *in vitro*. **A**, WT and IQGAP1$^{-/-}$ BM-derived macrophages (BMMs) were placed on upper Boyden chambers, and 100 ng/ml SDF-1α was placed in lower chambers for 4 hours. The number of migrated cells was counted and expressed as percent change vs. unstimulated WT cells (control) (n = 3, *$p<0.05$). **B**, Left, representative images of co-staining for anti-IQGAP1 (green) and Alexa Fluor 568 conjugated phalloidin (red) in WT-BMMs stimulated with SDF-1α (100 ng/mL, 2 min), as visualized by confocal microscopy. Arrows indicate colocalization of F-actin with IQGAP1 at the polarized plasma membrane in SDF-1α-stimulated BMMs. Phalloidin staining in IQGAP1$^{-/-}$ BMMs is shown in the right panels. Right, quantitative analysis of polarized F-actin in WT- and IQGAP1$^{-/-}$ BMMs, expressed as percentage of the total cell number at 16 different high power fields (×100)(*$p<0.05$). Bars show 20 μm. **C**, Adhesion capacity of bone marrow-derived macrophages (BMMs) to various extracellular matrixes. Cells were replated onto wells coated with fibronectin (FN), vitronectin (VN), fibrinogen (Fib), ICAM-1 or collagen IV (ColIV). After 30 minutes incubation, cells were washed by PBS gentry, fixed with 4% paraformaldehyde and stained with 0.05% crystal violet. Eluted dyes were measured by O.D. 590 nm. Data represents the means+/−SEM by duplicated samples and expressed as % cell adhesion vs. total input (*$p<0.05$).
doi:10.1371/journal.pone.0013440.g008

The present study also shows that ROS production in ischemic muscle, as well as "activated and tissue infiltrated" macrophage obtained by peritonitis inflammation model, is inhibited in IQGAP1$^{-/-}$ mice. We previously reported that ROS produced by NADPH oxidase expressed in inflammatory cells and ECs play a critical role in ischemia-induced neovascularization [11]. Moreover, IQGAP1 is shown to be involved in VEGF [18]- and hyperoxia [35]-induced ROS production in cultured ECs. Thus, the reduction of ROS at sites of inflammation and neovascularization in IQGAP1$^{-/-}$ mice may be at least due to a decrease in the number of infiltrated inflammatory cells and angiogenic ECs as well as their ROS producing capacity. A recent study reveals that a tissue gradient of ROS production represents a critical signal for recruiting leukocytes to injury sites *in vivo* [36]. Therefore, it is tempting to speculate that an IQGAP1-dependent increase in ROS signal from inflammatory cells and angiogenic ECs at ischemic sites may further facilitate the recruitment of monocytes/macrophages, thereby promoting revascularization and tissue repair/muscle regeneration.

To determine the mechanism by which IQGAP1 is involved in inflammatory cell recruitment, we examined the role of IQGAP1 in macrophage migration *in vitro*. IQGAP1 has been shown to cross-link actin filaments, and plays a key role in cell motility in various systems, including fibroblasts, cancer cells and ECs [15,16,18,20,22,37,38]. However, a role of IQGAP1 in the function of intact macrophages has not been investigated. Using cultured BM-derived macrophages (BMMs) derived from WT and IQGAP1$^{-/-}$ mice, the present study demonstrates that IQGAP1 is involved in macrophage migration in response to SDF-1α, but not to VEGF, thereby promoting macrophage infiltration to ischemic tissues. Given that macrophages mainly expresses VEGF receptor type 1 (VEGFR1) instead of VEGFR2, which is expressed in ECs, it is likely that IQGAP1 is coupled to VEGFR2 [18,19], but not to VEGFR1. In macrophages, IQGAP1 seems to be important mediator for SDF-1/CXCR4 signaling involved in cell migration. Investigating this point in detail is the subject of future studies. In ischemic tissues, expression of VEGF, but not SDF-1α, is reduced in IQGAP1$^{-/-}$ mice, which may contribute to impaired angiogenesis.

Mechanistically, IQGAP1 colocalizes with F-actin at the plasma membrane during active migration, and SDF-1α-induced actin polarization is inhibited in IQGAP1$^{-/-}$ BMMs. In line with these findings, we previously reported that IQGAP1 translocates to the leading edge where it colocalizes with VEGFR2 and NADPH oxidase in ECs, thereby promoting directional EC migration [18,20]. In RAW macrophage, IQGAP1 directly binds to Dia1 at the actin-rich phagocytic cup, which is required for migration and phagocytosis [17]. IQGAP1 also directly binds to the active form of Rac, Arp2/3 and N-WASP, thereby regulating actin reorganization in active migrating cells [13,15,16]. In addition, we found that the lack of IQGAP1 impairs fibronectin- or vitronectin-mediated macrophage adhesion. IQGAP1 association with β1 integrin has been reported previously [39]. Our results suggest that IQGAP1 may couple to other integrins to regulate macrophage adhesion. This point requires further investigation. Taken together, the present study indicates that IQGAP1 is involved in macrophage migration and adhesion, thereby promoting inflammatory cell infiltration into ischemic tissues, which may contribute to post-ischemic revascularization and tissue repair. It is possible that IQGAP1 expressed in inflammatory cells and/or ECs may regulate cross-talk between these cells, as reported for the role of neutrophil NADPH oxidase in activation of redox signaling in ECs [40] or endothelial IQGAP1 in lymphocyte transendothelial migration [41].

In summary, the present study provides compelling evidence that IQGAP1 plays a critical role in post-ischemic neovascularization and tissue repair by regulating inflammatory cell infiltration, EC-mediated angiogenesis and ROS production in ischemic tissues. We also found that IQGAP1-mediated recruitment of monocytes/macrophages into ischemic tissues is, in part, due to promoting their migration and adhesion capacity. These findings provide novel insight into IQGAP1 as a potential therapeutic target for inflammation- and angiogenesis-dependent ischemic diseases including peripheral vascular disease, arteriosclerosis, and wound healing, as well as tumor progression.

Supporting Information

Figure S1 Impaired regeneration as well as increased necrosis and fibrosis in ischemic muscles in IQGAP1$^{-/-}$ mice. A, Sections of muscles in lower limb were stained with hematoxyline and eosin (H/E). Regenerated myofibers which have centered nuclei (arrows) and ghost muscle cells devoid of nucleus (asterisk) are indicated. Adipocytes infiltration is indicated by arrow heads. The area of regeneration and necrosis including necrotic myofibers and infiltrated adipocytes are measured in tibialis anterior (TA) muscles which consistently show inflammation and necrotic damage in WT mice. B, serial sections of A were stained by Masson Trichrome. Blue indicates fibrosis area in TA muscles (n = 3-4, *p<0.05). Data shown are mean+/-SEM.
Found at: doi:10.1371/journal.pone.0013440.s001 (0.11 MB PDF)

Figure S2 A, Upper panel: representative dot plots of F4/80 and Ly-6C expression in CD11b^{+}/Ly-6G^{-} population WT and IQGAP1$^{-/-}$ mice in ischemic tibialis anterior muscles at day 4. Cell suspension was obtained from ischemic muscles using collagenase treatment and labeled with specific antibodies against CD45, CD11b, Ly-6C, Ly-6G and F4/80. Lower panel: total infiltrated cell numbers for pro-inflammatory M1 macrophages (CD11b^{+}Ly6G^{-}Ly6C^{+}F4/80^{+}; Ly-6C^{+} MP) and monocytes (CD11b^{+}Ly6G^{-}Ly6C^{+}F4/80^{-}; Ly-6C^{+} MO) as well as anti-inflammatory M2 macrophages (CD11b^{+}Ly6G^{-}Ly6C^{-}F4/80^{+}; Ly-6C^{-} MP) and monocytes (CD11b^{+}Ly6G^{-}Ly6C^{-}F4/80^{-}; Ly-6C^{-} MO) were calculated based on tissue weight and total cell numbers. Means+/-SEM from 2 different mice are shown. B, Pro-inflammatory M1 cytokines (TNFα and IL-6) and anti-inflammatory M2 cytokine (IL-10) expressions in ischemic muscles were measured by PCR analysis. Total RNA was extracted from muscle tissues and the data were normalized by GAPDH gene expression. Colony-stimulating factor receptor (c-fms) expression indicates macrophages infiltration. The relative gene expressions vs. WT are shown (n = 4 in each group, *p<0.05). C, Total cells collected from peritoneal cavities at 3 days after thioglycollate challenge were analyzed for CD11b, Ly-6G, Ly-6C and F4/80 expression by flow cytometry. The percentages of inflammatory (Ly-6C^{+}) monocytes (MO) or macrophages (MP) and antiinflammatory (Ly-6C^{-}) MO or MP were shown. Results represent the means+-SEM from 2 different mice in each group.
Found at: doi:10.1371/journal.pone.0013440.s002 (0.08 MB PDF)

Figure S3 A, Expression of CD11b (Mac-1) and F4/80 on cultured bone marrow-derived macrophages (BMMs). BMMs were stained with anti-CD11b and anti-F4/80 antibodies or isotype control antibodies and subjected to flow cytometric analysis. The values in right upper and right lower quadrants shows representative percentage of CD11b and F4/80 double positive, and CD11b positive but F4/80 negative in the total cells.